AD-A034 673 MASSACHUSETTS INST OF TECH CAMBRIDGE DEPT OF MECHANI--ETC F/G 9/5
MULTISTAGE HYDRAULIC SUMMING AND SIGNAL PROCESSING AMPLIFIERS A--ETC(U)
OCT 76 D LEE, D N WORMLEY DAAG39-73-C-0223

UNCLASSIFIED EPL-81202-1 HDL-CR-76-223-1 NL

| OF |
AD
A034673

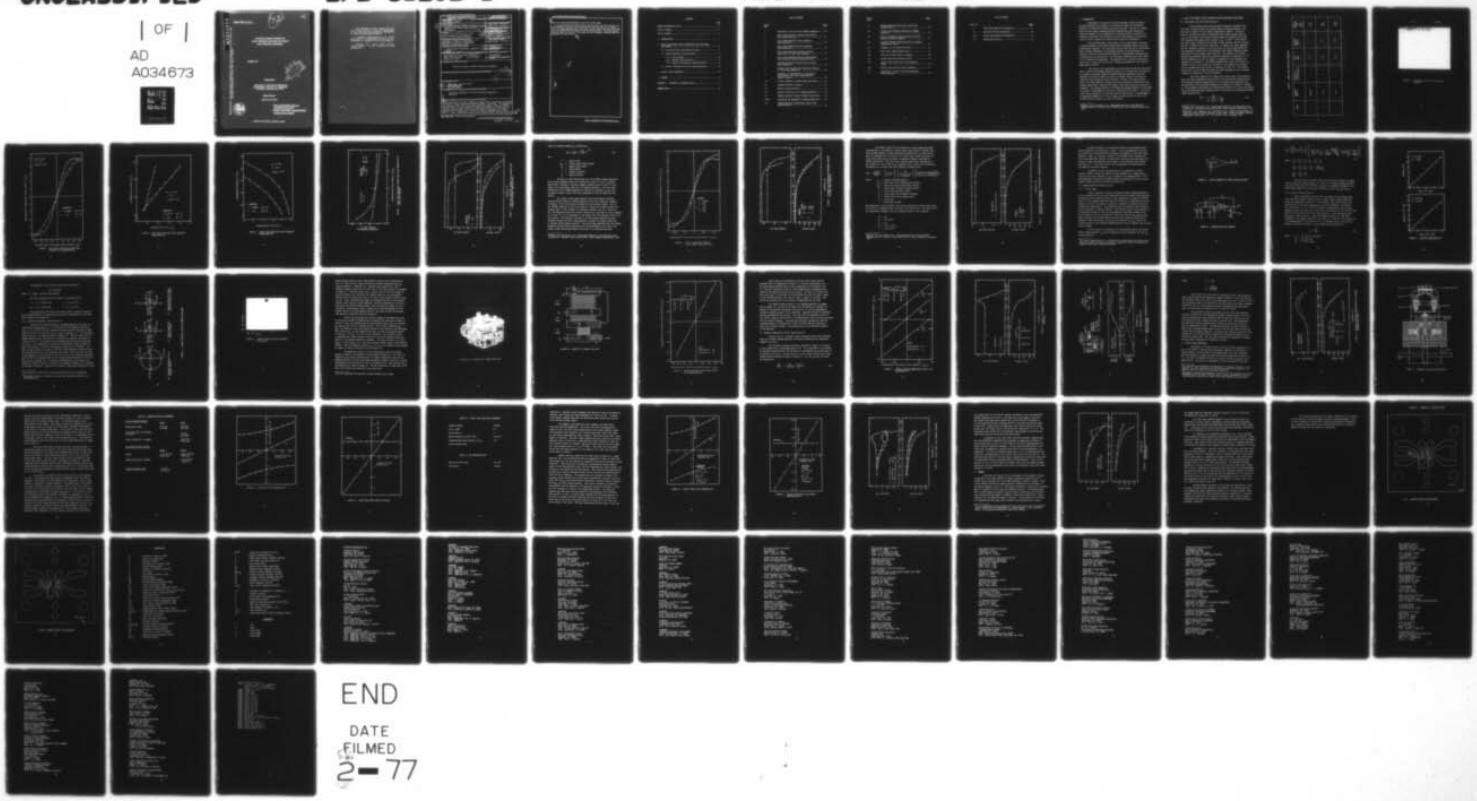

END

DATE
FILMED
2-77

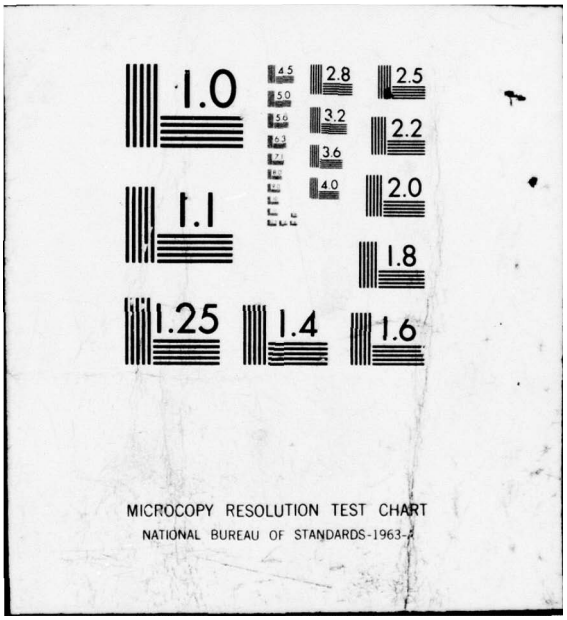
1.0
1.1
1.25
1.4
1.6
1.8
2.0
2.2
2.5
2.8
3.2
3.6
4.0
4.5
5.0
5.6
6.3
MICROCOPY RESOLUTION TEST CHART
NATIONAL BUREAU OF STANDARDS-1963-A

HDL-CR-76-223-1

12

FC

MULTISTAGE HYDRAULIC SUMMING AND SIGNAL PROCESSING AMPLIFIERS AND FLUIDIC INPUT SERVOVALVE DEVELOPMENT

OCTOBER 1976

Prepared by

Department of Mechanical Engineering
Massachusetts Institute of Technology
Cambridge, Massachusetts 02139

Under Contract

DAAG-39-73-C-0223

U.S. Army Material Development and Readiness Command
HARRY DIAMOND LABORATORIES
Adelphi, Maryland 20783

The findings in this report are not to be construed as an official Department of the Army position unless so designated by other authorized documents.

Citation of manufacturers' or trade names does not constitute an official indorsement or approval of the use thereof.

Destroy this report when it is no longer needed. Do not return it to the originator.

SECURITY CLASSIFICATION OF THIS PAGE (When Data Entered)

REPORT DOCUMENTATION PAGE

READ INSTRUCTIONS BEFORE COMPLETING FORM

1. REPORT NUMBER: HDL-CR-76-223-1	2. GOVT ACCESSION NO.
3. RECIPIENT'S CATALOG NUMBER	
4. TITLE (and Subtitle): Multistage Hydraulic Summing and Signal Processing Amplifiers and Fluidic Input Servovalve Development.	5. TYPE OF REPORT & PERIOD COVERED: Final rept.
6. PERFORMING ORG. REPORT NUMBER: EPL-81202-1	
7. AUTHOR(s): David Lee, David N. Wormley	8. CONTRACT OR GRANT NUMBER(s): DAAG-39-73-C-0223 NEW; PRON: A1-4-R-0002-03-A1-A-9
9. PERFORMING ORGANIZATION NAME AND ADDRESS: Department of Mechanical Engineering, Massachusetts Institute of Technology, Cambridge, Massachusetts 02139	10. PROGRAM ELEMENT, PROJECT, TASK AREA & WORK UNIT NUMBERS: Program Element: 6.11.02.A
11. CONTROLLING OFFICE NAME AND ADDRESS: U.S. Army Materiel Development & Readiness Command, Alexandria, Va. 22333	12. REPORT DATE: October 1976; 13. NUMBER OF PAGES: 55
14. MONITORING AGENCY NAME & ADDRESS (if different from Controlling Office): Harry Diamond Laboratories, 2800 Powder Mill Road, Adelphi, MD. 20783	15. SECURITY CLASS. (of this report): UNCLASSIFIED; 15a. DECLASSIFICATION/DOWNGRADING SCHEDULE

16. DISTRIBUTION STATEMENT (of this Report)

Approved for public release; distribution unlimited.

17. DISTRIBUTION STATEMENT (of the abstract entered in Block 20, if different from Report)

18. SUPPLEMENTARY NOTES

DRCMS Code: 611102.11.71200
1T161102A33B
HDL Proj: 302431

19. KEY WORDS (Continue on reverse side if necessary and identify by block number)

Proportional Amplifier, Gain Block, Hydraulic Amplifiers, Servovalve

20. ABSTRACT (Continue on reverse side if necessary and identify by block number)

The development of fluidic summing and dynamic signal compensation operational amplifiers for high performance hydraulic systems is described. The amplifiers are constructed from three stage fluid amplifiers using as input and feedback elements linear resistors constructed from small diameter to length ratio tubing and capacitors constructed from flexible metal diaphragms. The summing amplifier has a pressure gain of 50 and a frequency response which is flat to 100 Hz. Dynamic compensation elements were constructed with lead-lag action

OVER

DD FORM 1 JAN 73 1473 EDITION OF 1 NOV 65 IS OBSOLETE

220 022 LB

where the lead action dominates in the 20 to 40 Hz range.

A four-way fluidic input servovalve has been developed. The valve consists of a fluid amplifier driving a pair of bellows that act directly on the flapper of the first stage flapper-nozzle valve, and a second stage spool valve whose position is controlled by the output of the first stage valve. The valve accepts pressure inputs in the 0 to 7 kPa range and has a frequency response which has decreased by 3 dB at 30 Hz.

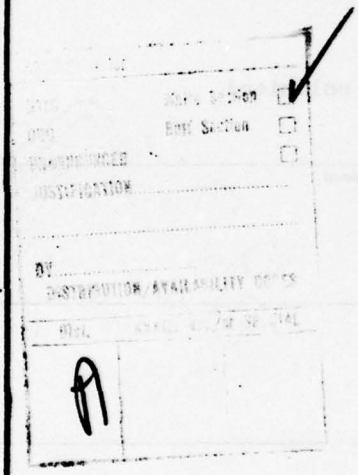

CONTENTS

LIST OF FIGURES

LIST OF TABLES

1. INTRODUCTION

Development of effective pure fluid sensing, signal processing and power amplification elements can effectively extend the performance capability of hydraulic actuation and control systems. The use of a common fluid for both signal sensing/processing elements and power modulation/actuation elements and the elimination of electro-hydraulic interfaces increases the potential for application of pure fluid systems in systems subjected to severe temperature, radiation and vibration environments.

The work described in this report is the second phase of research to develop hydraulic pure fluid sensing-signal processing elements and power amplification elements. The first phase of this work[1] has led to the development of design techniques for multistage hydraulic fluid amplifiers for pressure, flow and/or power gain applications. These design techniques were illustrated in the construction of a three stage amplifier with output power of 42 W from HDL 2-2B laminates. The amplifier has a blocked load pressure gain of 325, a power gain of 825 and a frequency response with less than 90° phase shift at 80 Hz.

The focus of the second phase of work has been directed to two areas. First, using the multistage amplifier design as a starting point, multiple input summing and dynamic signal processing hydraulic amplifiers have been developed to provide a basis for static and dynamic signal processing required in high performance control systems. Second, a four-way, fluidic input, two stage hydraulic servovalve has been developed to provide the link between signal power levels and the higher power level modulation required for actuators. The characteristics of the signal processing elements are described in Section 2; development of the valve is described in Section 3. In all the tests results described, the working fluid has been Univis J-43 maintained at an operating temperature of 27°C at which the fluid density is 8.69×10^2 N-s^2/m^4 and the viscosity is 1.88×10^{-2} N-s/m^2.

---

[1] Wormley, D.N. and Wilson, D.R., "Multistage Hydraulic Fluid Amplifier Characteristics," Technical Report HDL-TR-156-1, Harry Diamond Laboratories, 1974.

2. STATIC AND DYNAMIC SIGNAL PROCESSING USING MULTISTAGE GAIN BLOCKS

2.1 Multistage Gain Block Characteristics

The multistage gain block described by Wormley and Wilson[1] has been used to develop static and dynamic signal processing elements. The gain block consists of three stages, summarized in Table I. The first stage is constructed of HDL 2-2B laminates with a supply nozzle width of b_s = 0.5 mm, whereas the second and third stages are constructed with HDL 2-2B laminates with supply nozzle widths of b_s = 1.0 mm.[1] In the second and third stages, laminates were stacked to form sections, and the sections were put in parallel to form an amplifier. To improve the input impedance and the frequency response of the gain block, the first stage design has been modified by replacing the 2-2B laminates with 231004A laminates, while the second and third stages remain the same. The design of the 231004A laminate was performed using the techniques described by Drzewiecki et al.[2] The two laminates are shown in Figure 1; dimensions of the laminates are summarized in Appendix A. The 231004A laminate has control ports that are reduced in size at the supply port interface, a new supply nozzle design and an increased size vent region in comparison to the 2-2B. This smaller control port in the 231004A increases its input impedance and its frequency response in comparison to the 2-2B laminate.

Test data comparing the blocked load pressure gain characteristics, input and output impedance characteristics, bias sensitivity characteristics and frequency response characteristics of the single stage amplifiers constructed from 2-2B and 231004A laminates are summarized in Figures 2 through 6. The parameters specifying the configurations tested are cited in the figures where the operating supply pressure level is specified by the modified Reynolds number N_R' defined as:

$$N_R' = \frac{N_R}{(1 + \frac{1}{\sigma})^2 (1 + \frac{x_{th}}{b_s})} \qquad (1)$$

---

[1] Wormley, D.N. and Wilson, D.R., "Multistage Hydraulic Fluid Amplifier Characteristics," Technical Report HDL-TR-156-1, Harry Diamond Laboratories, 1974.

[2] Drzewiecki, T.M., Wormley, D.N., and Manion, F.M., "Computer-Aided Design Procedure for Laminar Fluidic Systems," Trans. ASME, Journal of Dynamic Systems, Measurement, and Control, Vol. 97, Series G, No. 4, December 1975.

TABLE I. THREE STAGE AMPLIFIER PARAMETERS

Stage	Laminate Design	Number of Sections to Form Amplifier	Size, b_s (mm)	Section Aspect Ratio, σ	Supply Pressure, P_s (kPa) [psi]
1	231004A	1	0.5	2	110 [16]
2	2-2B	2	1.0	0.5	661 [96]
3	2-2B	8	1.0	0.25	3970 [576]

2-2B 231004A

FIGURE 1. PHOTOGRAPH OF THE 2-2B AND 231004A LAMINATES

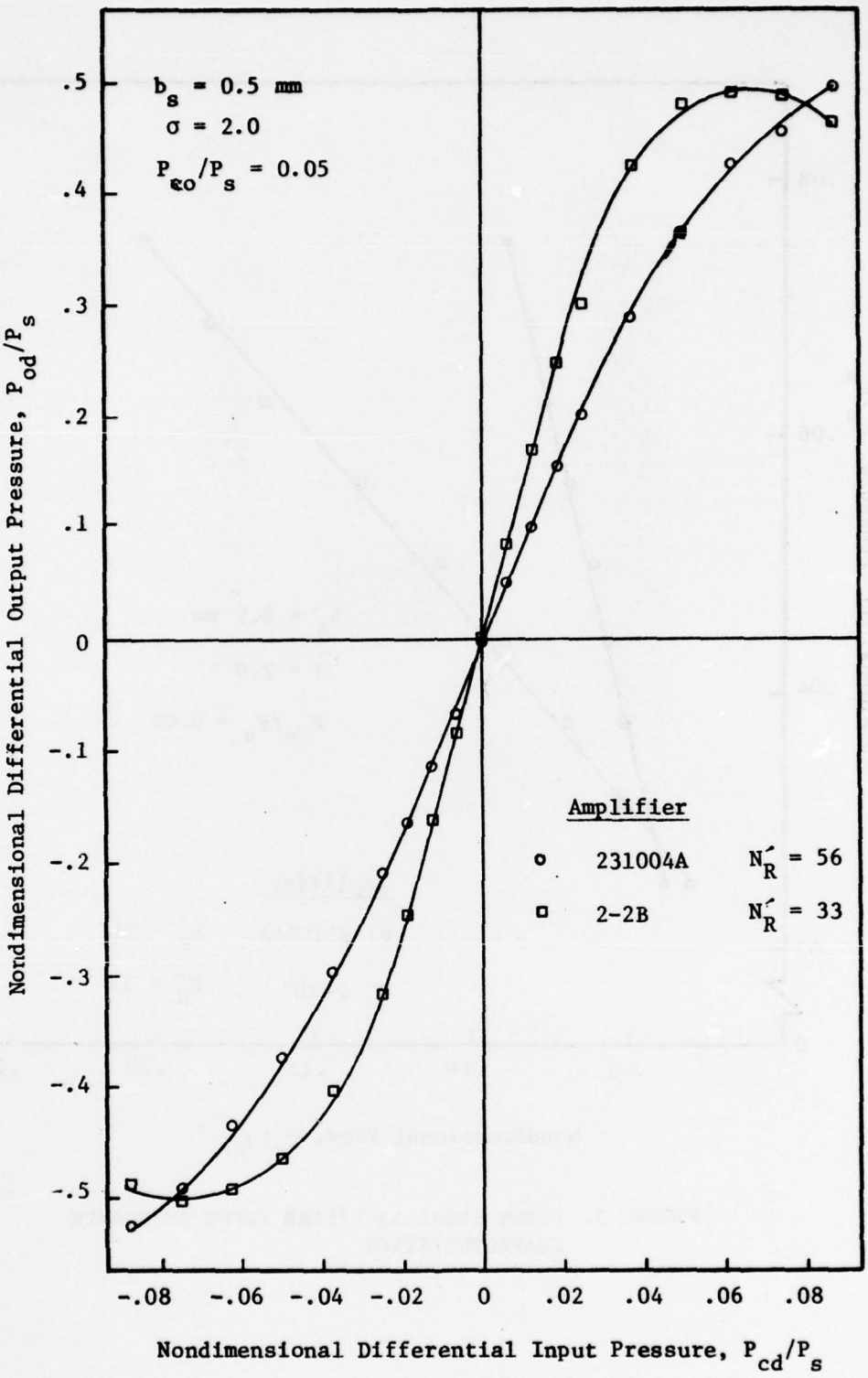

FIGURE 2. FIRST STAGE AMPLIFIER BLOCKED LOAD PRESSURE GAIN CHARACTERISTICS

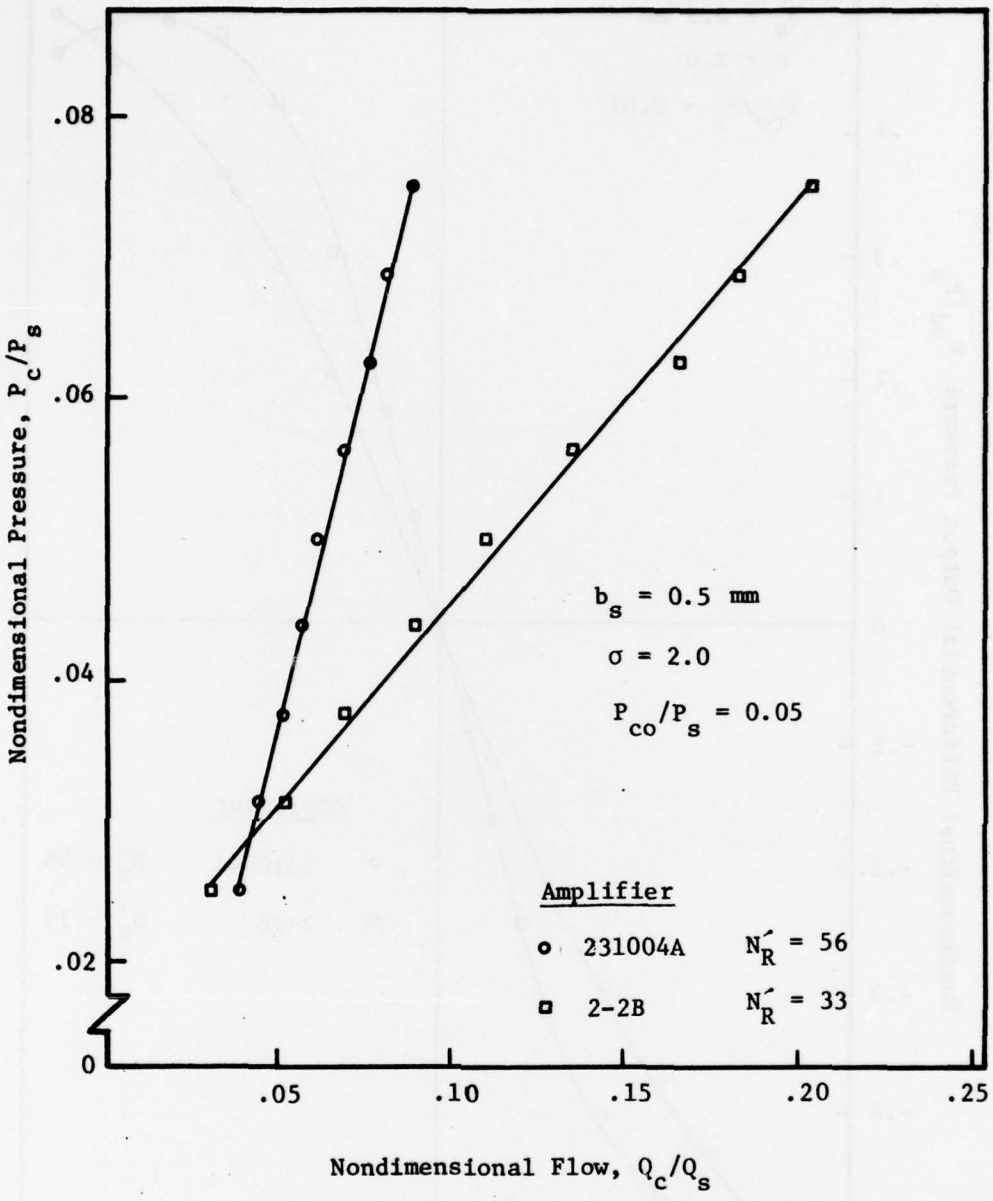

FIGURE 3. FIRST STAGE AMPLIFIER INPUT IMPEDANCE CHARACTERISTICS

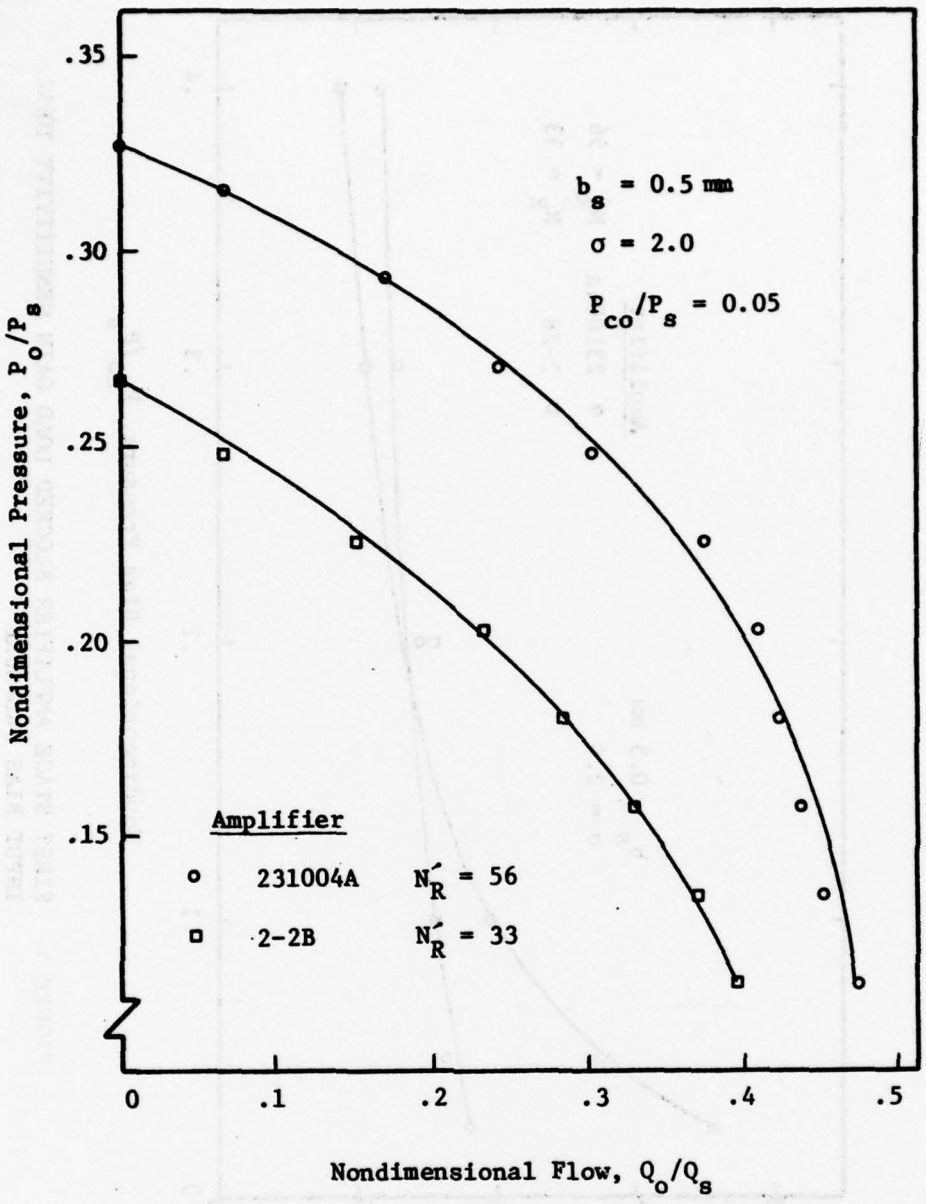

FIGURE 4. FIRST STAGE AMPLIFIER OUTPUT IMPEDANCE CHARACTERISTICS

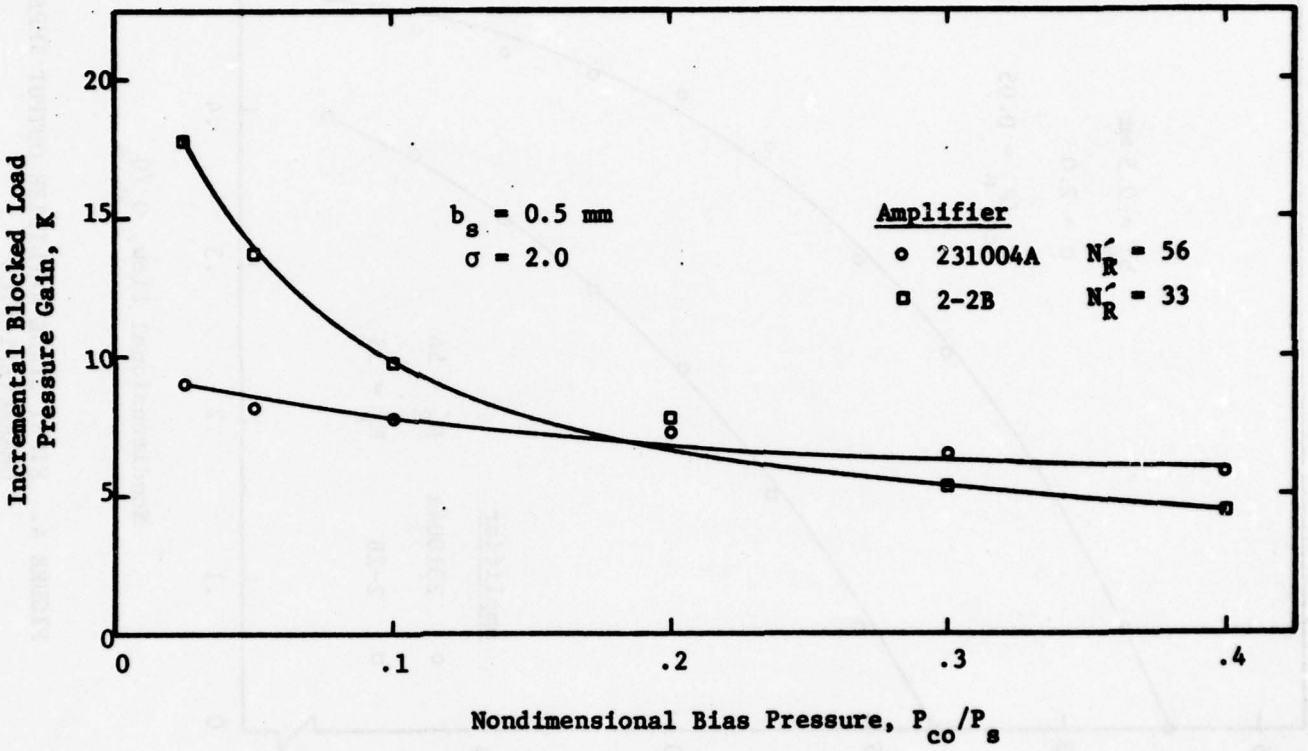

FIGURE 5. FIRST STAGE AMPLIFIER BLOCKED LOAD GAIN SENSITIVITY TO INPUT BIAS PRESSURE

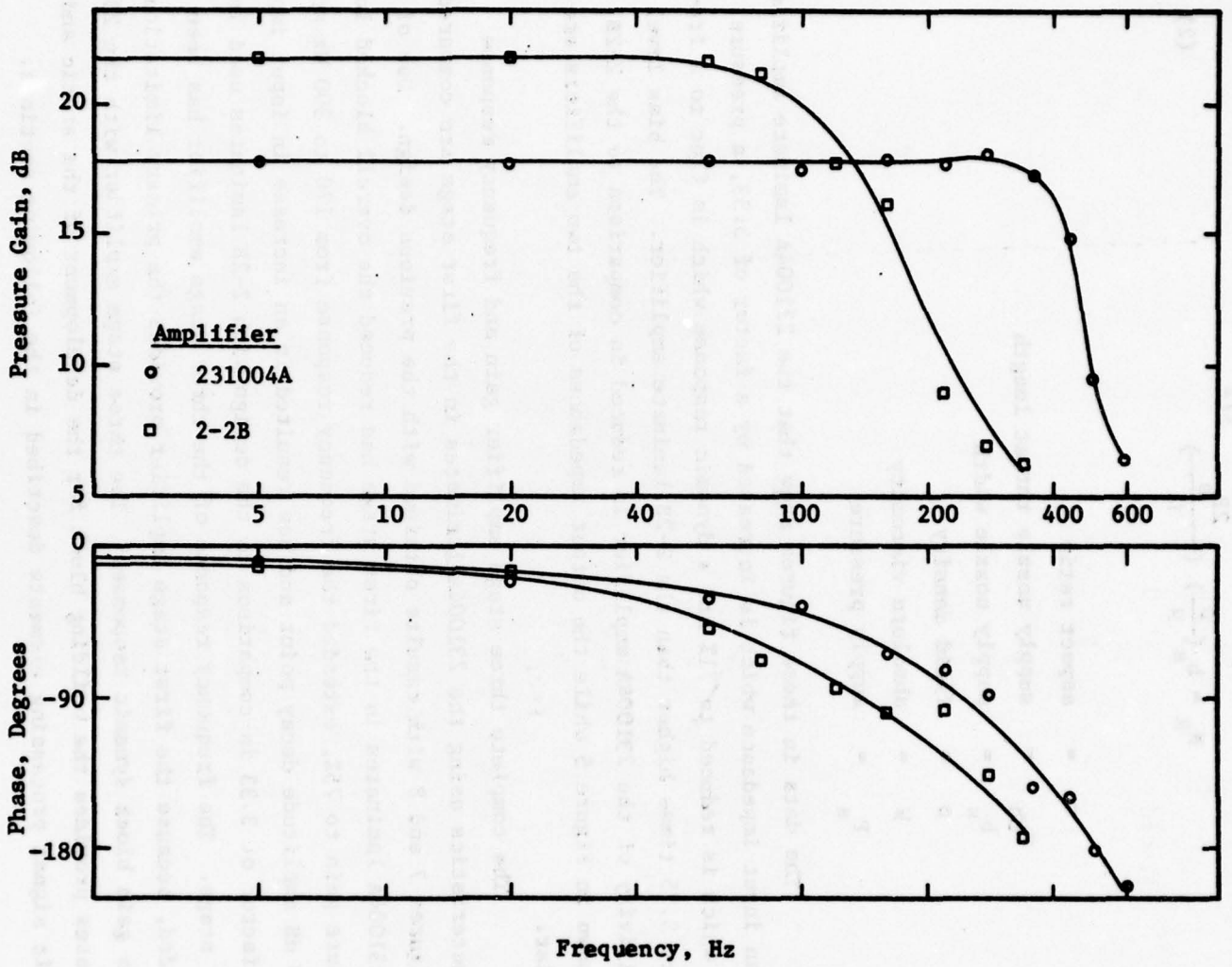

FIGURE 6. FIRST STAGE AMPLIFIER BLOCKED LOAD PRESSURE GAIN FREQUENCY RESPONSE CHARACTERISTICS

where the Reynolds number N_R is defined as:

$$N_R = b_s \left(\frac{\rho}{\mu}\right) \left(\frac{2P_s}{\rho}\right)^{1/2} \qquad (2)$$

and

σ = aspect ratio

x_{th} = supply nozzle throat length

b_s = supply nozzle width

ρ = fluid density

μ = absolute viscosity

P_s = supply pressure

The data in these figures show that the 231004A laminate amplifier has an input impedance which is increased by a factor of 3.33, a pressure gain which is reduced to 71% and a dynamic response which is flat to a frequency 3.75 times higher than the 2-2B laminate amplifier. The bias level sensitivity of the 231004A amplifier is reduced in comparison to the 2-2B as shown in Figure 5 while the output impedances of the two amplifiers are similar.

The complete three stage amplifier gain and frequency response characteristics using the 231004A laminates in the first stage are compared in Figures 7 and 8 with results obtained with the previous design. Use of the 231004A laminates in the first stage has reduced the overall blocked load pressure gain to 75%, extended the frequency response from 170 to 300 Hz at the 3 dB amplitude decay point and has resulted in an increase in input impedance by a factor of 3.33 in comparison to the design with 2-2B laminates used in the first stage. The frequency response of the three stage amplifier has been extended, because the first stage amplifier provides the primary limitation to the gain block dynamic response.[1] The three stage amplifier with the 231004A laminates provides the building block for the development of the static and dynamic signal processing elements described in the following sections.

---

[1] Wormley, D.N. and Wilson, D.R., "Multistage Hydraulic Fluid Amplifier Characteristics," Technical Report HDL-TR-156-1, Harry Diamond Laboratories, 1974.

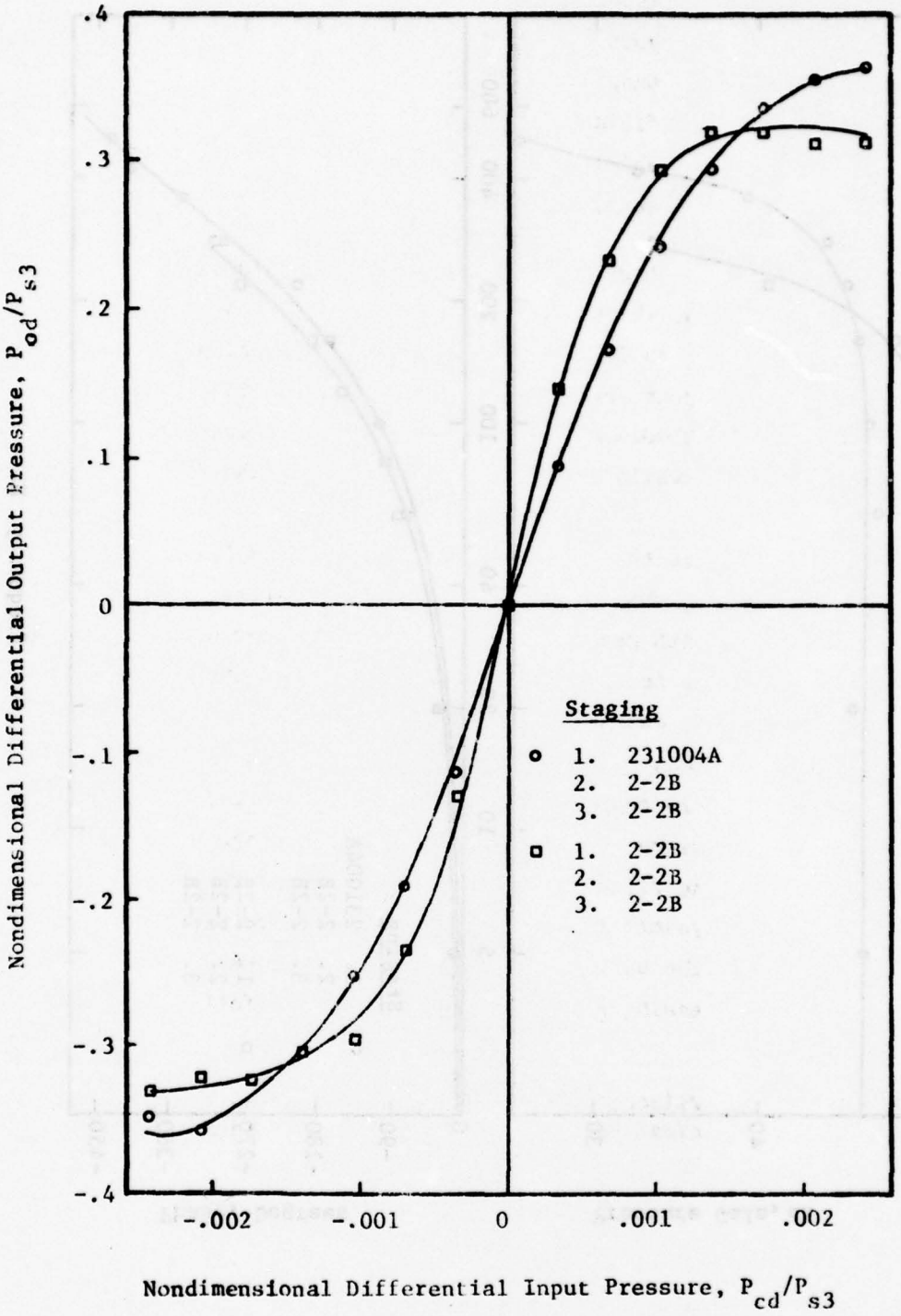

FIGURE 7. BLOCKED LOAD STATIC PRESSURE GAIN OF THREE STAGE AMPLIFIER

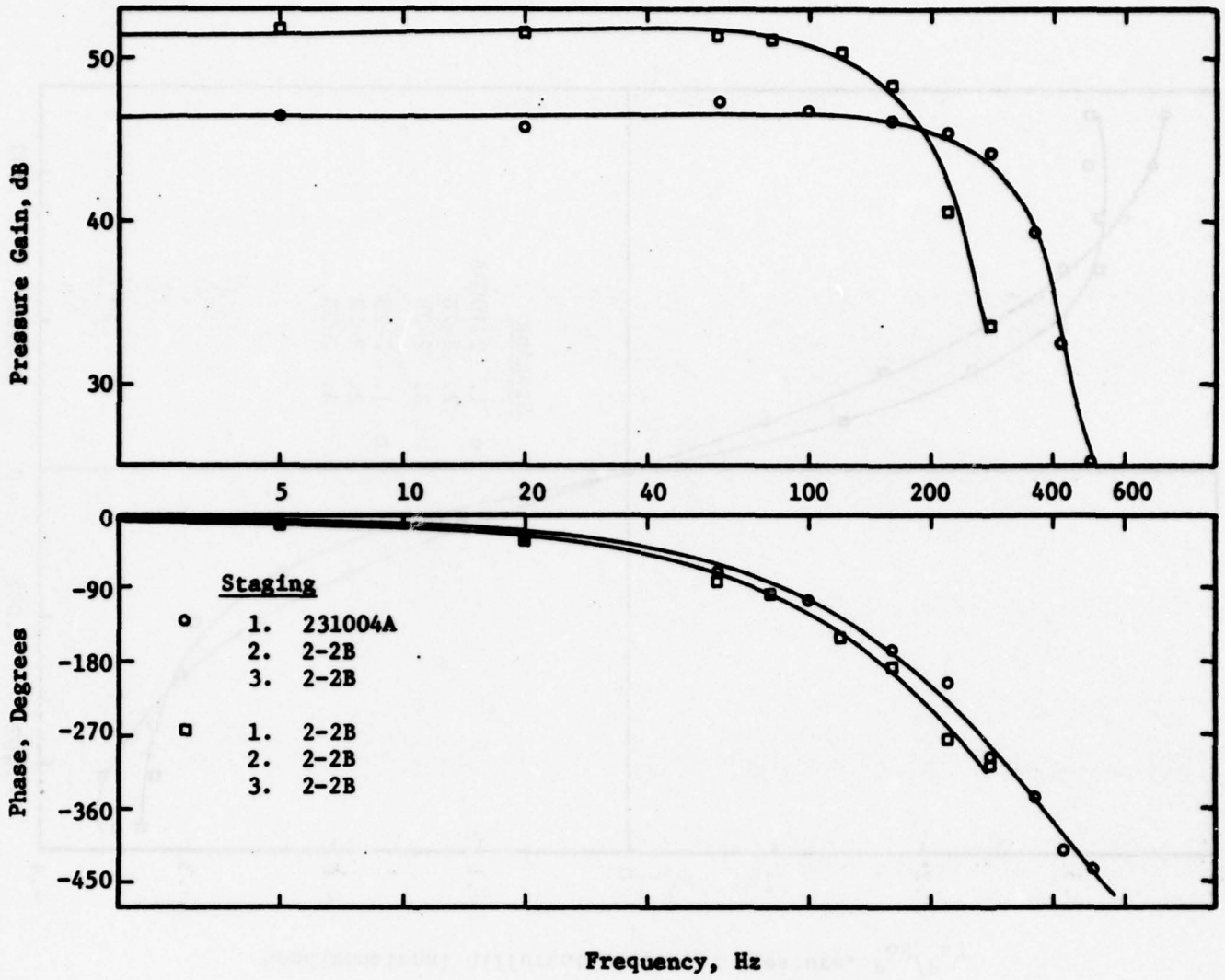

FIGURE 8. BLOCKED LOAD PRESSURE GAIN FREQUENCY RESONSE OF THREE STAGE AMPLIFIER

To provide a basis for the analysis of circuits using the three stage amplifier, the amplifier dynamic output-input pressure transfer function has been modeled for small amplitude disturbances as a linear system which is represented as the product of a third order transfer function and a pure delay based upon an analysis of amplifier dynamics described by Wormley and Wilson.[1] The third order transfer function is represented as the product of a first order and a quadratic factor, while the pure delay is represented as a second order Padé expansion as shown below:

$$T(s) = \frac{P_{od}(s)}{P_{cd}(s)} = -\left[\frac{K}{T_1 s + 1}\right] \cdot \left[\frac{\omega_n^2}{s^2+2\xi\omega_n s+\omega_n^2}\right] \cdot \left[\frac{1-0.5\tau s + 0.125(\tau s)^2}{1+0.5\,\tau s + 0.125(\tau s)^2}\right] \quad (3)$$

where:

s = Laplace Transform Operator

P_{od} = gain block output differential pressure

P_{cd} = gain block input differential pressure

T = output-input pressure transfer function

T_1 = first order lag time constant

ω_n = second order factor natural frequency

ξ = second order factor damping ratio

K = static gain

τ = delay time constant

The parameters in this transfer function were obtained by fitting this transfer function to measured data for the three stage gain block. The degree of fit is illustrated in Figure 9 for the following values of the constants:

K = 215

ω_n = 1634 rad/s

ξ = 0.6

T_1 = 6.12×10^{-4} s

τ = 1.33×10^{-3} s

---

[1] Wormley, D.N. and Wilson, D.R., "Multistage Hydraulic Fluid Amplifier Characteristics," Technical Report HDL-TR-156-1, Harry Diamond Laboratories, 1974.

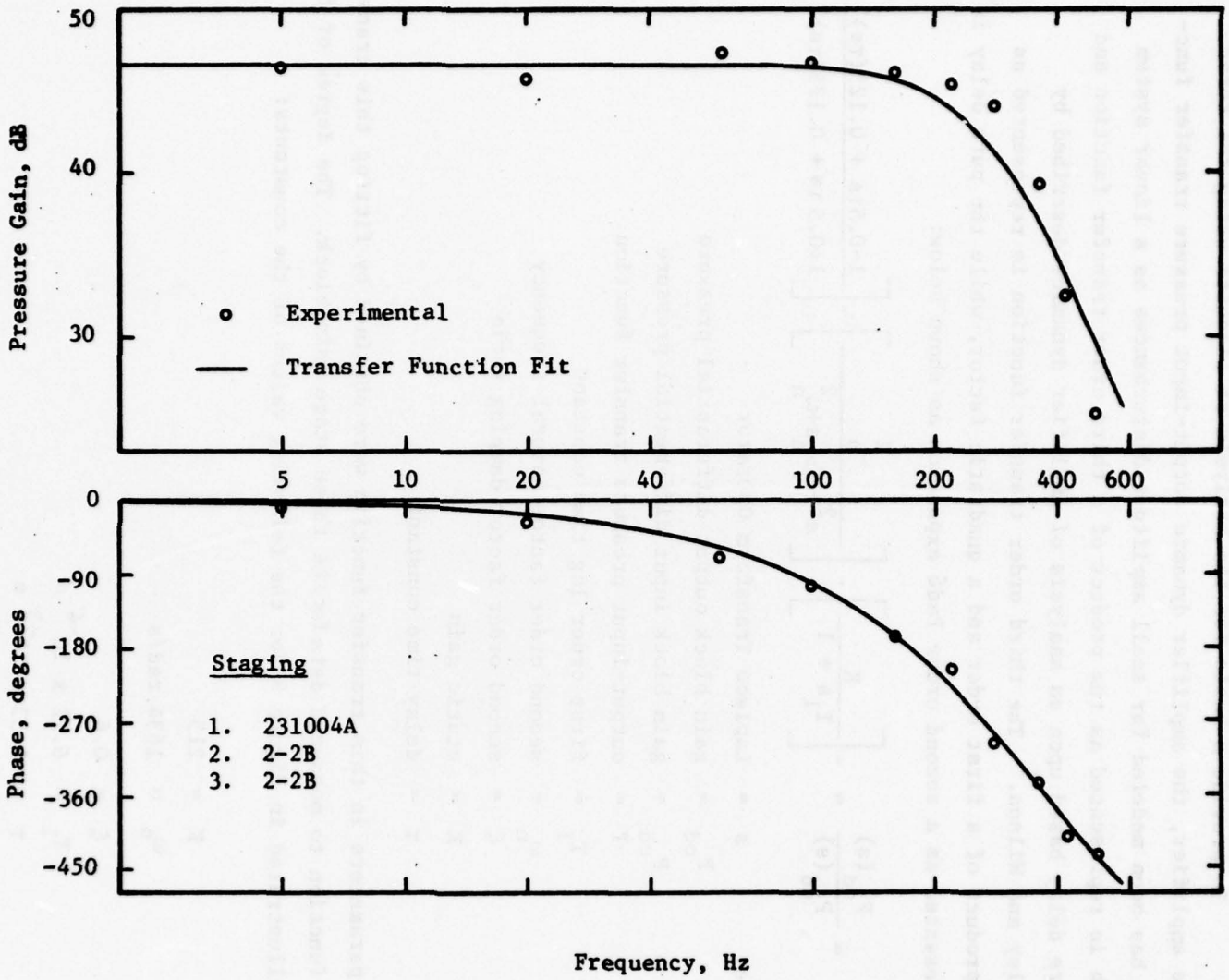

Figure 9. COMPARISON OF EXPERIMENTAL AND ANALYTICAL APPROXIMATION FOR THREE STAGE AMPLIFIER DYNAMIC RESPONSE

As shown in Figure 9, the agreement between the experimental data and the analytical representation is good. In the representation, the first and second order terms effectively represent the dynamics of the first stage amplifier, since its frequency response is the primary factor limiting the three stage amplifier; however, in addition to the delay time associated with the first stage, the additional delay times of the second and third stages contribute to τ. This delay term at 190 Hz contributes 90° phase shift to the amplifier frequency response.

A schematic circuit representation of the amplifier is illustrated in Figure 10 where the amplifier input impedance Z_a, transfer function T(s) and output impedance Z_o are included in the representation.* This representation is used for preliminary design calculations in the static and dynamic signal processing circuits described below.

2.2 Summing Amplifier Characteristics

2.2.1 Circuit Model

A basic component of signal processing systems, summing amplifiers, can be constructed from the three stage gain block and passive fluid resistors. The general circuit shown in Figure 11 was considered as a basis for development of a fluid summing amplifier where each resistor is represented by an impedance Z, so that the effects of parasitic inertance in resistors can be included where appropriate.* The resistors Z_1 and Z_2 represent input resistors and Z_f represents a feedback resistor. The resistor Z_g has been included in the generalized model so that the nondimensional input bias pressure level may be adjusted to 5% at the amplifier, while the resistors Z_{D1} and Z_{D2} have been provided so that both feedback pressure levels and bias levels may be adjusted. When the resistors Z_g and Z_{D2} are infinite and Z_{D1} is zero, the circuit reduces to the standard summing amplifier circuit commonly used in electronic systems.

For the circuit as configured, the relationship between the differential output pressure P_{od} and the differential input pressures, P_{1d} and P_{2d} can be derived as:

---

*The circuit representation is a differential representation which shows half the actual number of physical components. Signals are shown as differential signals rather than single sided signals.

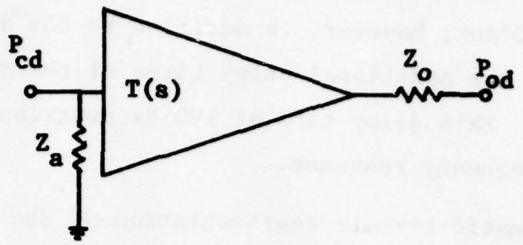

FIGURE 10. CIRCUIT SCHEMATIC OF THREE STAGE GAIN BLOCK

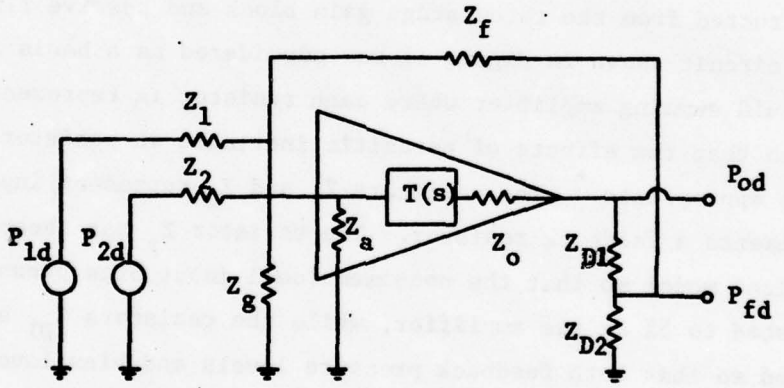

FIGURE 11. SUMMING AMPLIFIER SCHEMATIC

$$P_{od} = -\left[\frac{Z_f}{Z_1} P_{1d} + \frac{Z_f}{Z_2} P_{2d}\right] \cdot \left[\frac{T(s)\, R^*}{\frac{Z_f Z_o}{Z_{D1}} R^{**}\left(\frac{1}{Z_{D1}} + \frac{Z_o}{Z_f T Z_{DO}}\right) - \frac{Z_f Z_o}{Z_{D0}} + R^* R^{**}\left(\frac{T}{Z_{D1}} + \frac{Z_o}{Z_f Z_{DO}}\right)}\right] \tag{4}$$

where: $$\frac{1}{R^*} = \frac{1}{Z_g} + \frac{1}{Z_a} + \frac{1}{Z_1} + \frac{1}{Z_2} + \frac{1}{Z_f}$$

$$\frac{1}{R^{**}} = \frac{1}{Z_{D2}} + \frac{1}{Z_{D1}} + \frac{1}{Z_f} + \frac{Z_o}{Z_f T(s) Z_{D1}}$$

$$\frac{1}{Z_{D0}} = \frac{1}{Z_{D1}} + \frac{1}{Z_o}$$

The first term in brackets shows that the output pressure is simply a sum of $[Z_f/Z_1]P_{1d}$ and $[Z_f/Z_2]P_{2d}$ as occurs in a classical summing amplifier. The second term in brackets reflects the effects of amplifier dynamics, T(s), finite input impedance Z_a and output impedance Z_o and of Z_g, Z_{D1} and Z_{D2}.

2.2.2 Resistor Characteristics

Input and feedback resistors were developed for the summing amplifier from small diameter stainless steel tubing. These resistor characteristics are summarized in Figure 12. The resistors have nearly linear characteristics for the range of pressures and flows considered. One resistor has a resistance $R = 1.5 \times 10^{10}$ N-s/m^5 which is approximately equal to the amplifier input resistance, while the second resistor has $R = 1.4 \times 10^{12}$ N-s/m^5 which is 93 times the value of the input resistor. These resistances were selected as target values for input and feedback resistors so that input pressures to the summing amplifier were in the 0 to 7 kPa (0-1 psi) range with a 5% nondimensionalized pressure bias at the amplifier input. For each resistor the parasitic inertance I_i was estimated from slug flow as:

$$I_i = \frac{\rho \ell_i}{A_i} \tag{5}$$

where: I_i = i^{th} resistor inertance
A_i = i^{th} tube area
ℓ_i = i^{th} tube length

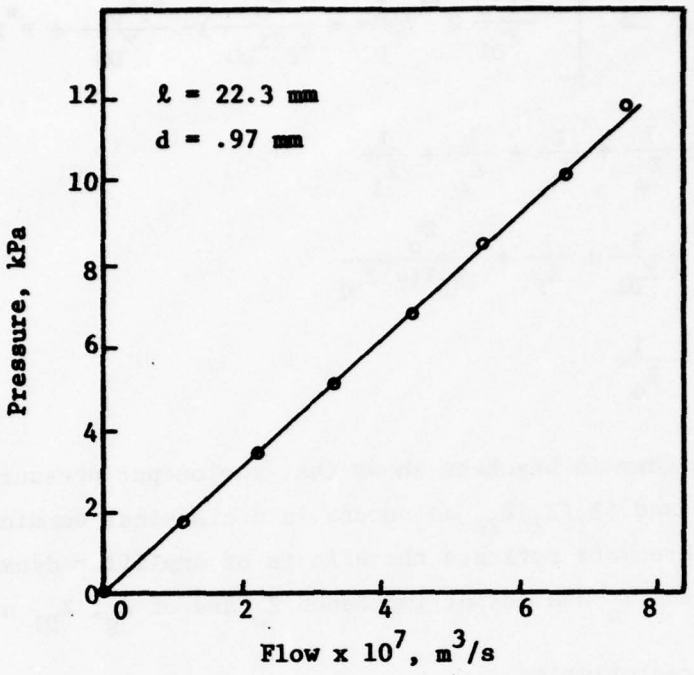

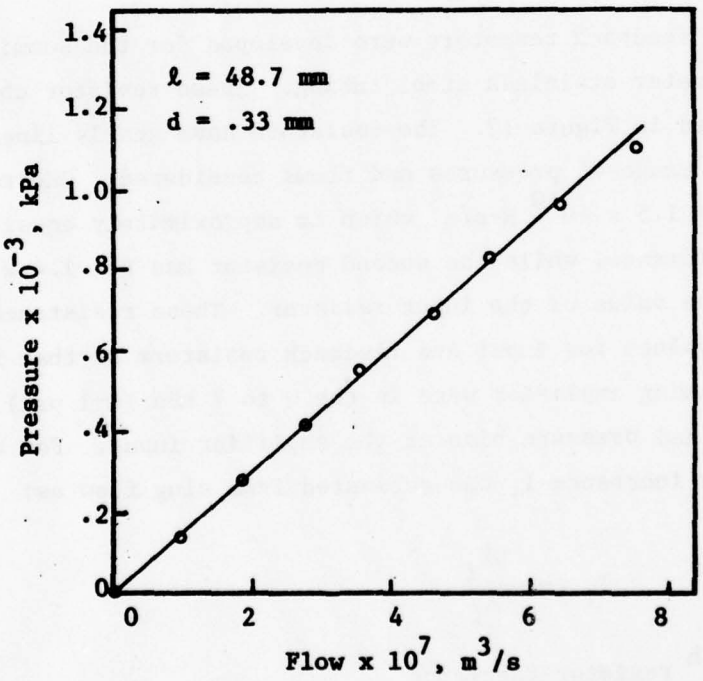

FIGURE 12. RESISTOR CHARACTERISTICS

The impedance of each resistor can then be written as:

$$Z_i = R_i(\tau_i s+1)$$

where: $\tau_i = I_i/R_i$ = resistor time constant

The time constants for each resistor is tabulated below:

$R = 1.5 \times 10^{10}$ N-s/m^5 $\qquad \tau = 1.78 \times 10^{-3}$ s

$R = 1.4 \times 10^{12}$ N-s/m^5 $\qquad \tau = 3.4 \times 10^{-4}$ s

For frequencies below 90 Hz, the input resistor parasitic inertance may be neglected while for frequencies below 450 Hz the inertance of the feedback resistor may be neglected.

2.2.3 Amplifier Performance Characteristics

The stability characteristics of a summing amplifier with input resistances R_1 and R_2 equal to 1.5×10^{10} N-s/m^5 and the feedback resistor R_f equal to 1.4×10^{12} N-s/m^5 were computed using the transfer functions of equations (3) and (4) for the case of $R_g = \infty$, $R_{D2} = \infty$ and $R_{D1} = 0$.* The resulting Nyquist plot for the system is shown in Figure 13.** The plot shows that the summing amplifier with the resistors as specified is unstable and should oscillate at 193 Hz. The amplifier with resistances specified was constructed and tested. The amplifier was unstable and oscillated as shown in Figure 14 where the frequency is 189 Hz, which agrees closely with the analysis. The peak to peak pressures are equal to the three stage amplifier saturation level. The principal reason for this instability is that at 190 Hz the open loop gain of the amplifier is nearly equal to its static value, while the open loop phase shift is 180° with approximately 90° of the phase shift attributed to the pure delay term in equation (3). To stabilize the amplifier in its present configuration requires either an increase in the feedback resistance or a decrease in the input resistance. Because of the desire to keep input resistors at their

---

*The inertance of each resistor was included in the resistor impedances.

**Encirclement of the -1.0 point on the real axis indicates instability in the Nyquist plot.

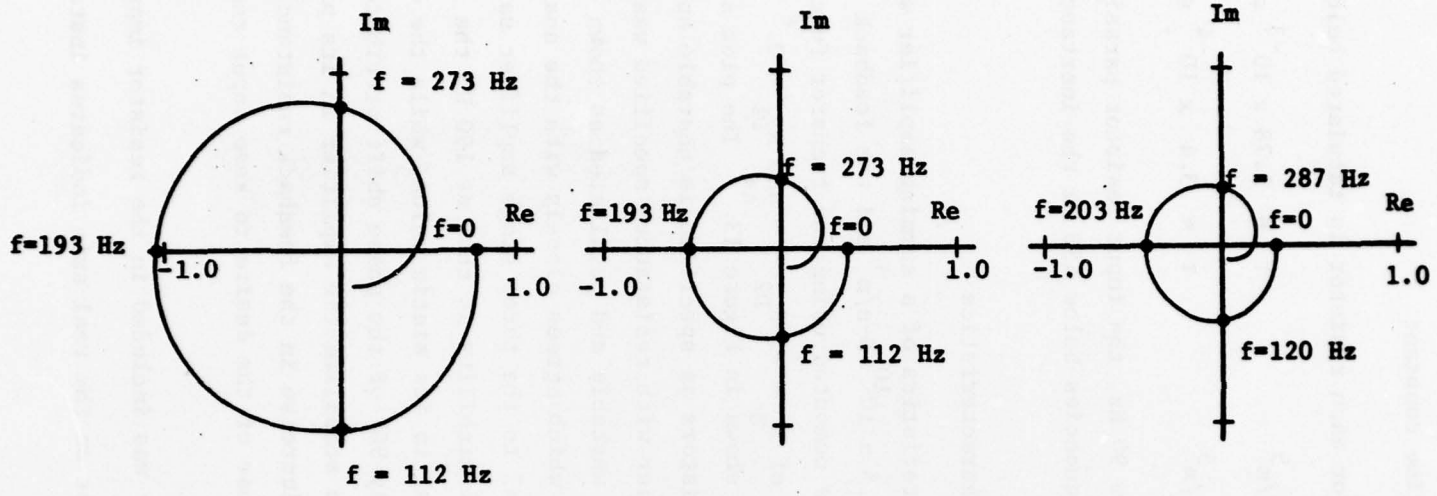

(a) Unstable System with Base Feedback Resistor

(b) Stable System with Pressure Divider

(c) Stable System with Base Feedback Resistor Doubled

FIGURE 13. NYQUIST STABILITY PLOT OF SUMMING AMPLIFIER

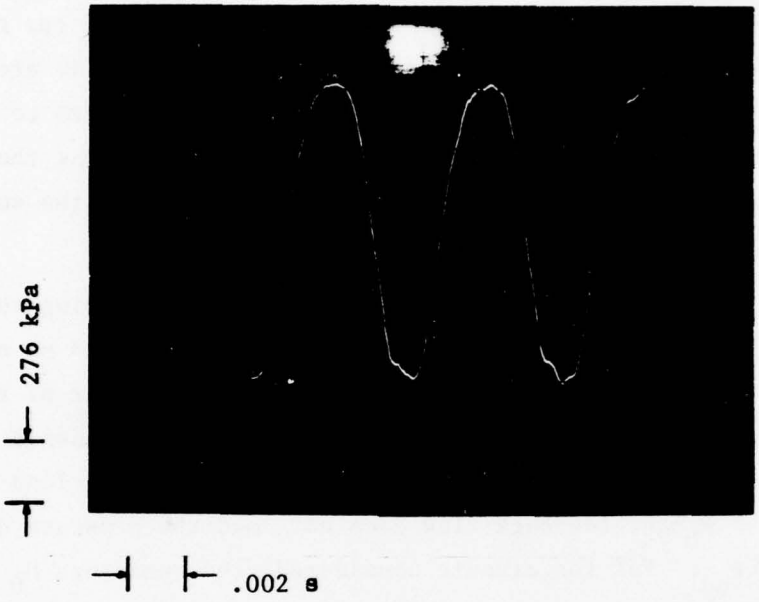

FIGURE 14. SUMMING AMPLIFIER OUTPUT PRESSURE OSCILLATION

design nominal values so that input pressure levels could be maintained in the 0 to 7 kPa (1-0 psi) range, altering the feedback resistance was considered primarily. A Nyquist plot, computed using equation (4), with a capillary resistor whose value is twice that of the base resistor is presented in Figure 13.* This data shows that a resistor that is twice the length of the base resistor will stabilize the feedback amplifier, or alternately a resistor which is seventy per cent of the area of the original resistor could be used. While increasing the length or decreasing the area of the feedback resistor could provide a stable amplifier, neither alternative is attractive. Increasing the resistor length yields a tube of sufficient length to be inconvenient in maintaining a small, compact unit, while decreasing the area further results in a tube diameter which is less than one half the smallest flow dimension associated with the amplifiers.

Rather than increasing the resistor length or decreasing the area, an alternative method of stabilizing the amplifier has been used as shown in Figure 11, where the feedback path has been modified with a pair of resistors R_{D1} and R_{D2} that act as a pressure divider. For the case considered $R_{D1} = R_{D2} = R_D$. When $R_D >> R_o$, the pressure divider circuit does not load the amplifier and when $R_f >> R_D$ the feedback flow does not load the pressure divider so that $P_{fd} = 1/2\ P_{od}$. For the circuit considered, the resistors R_D were constructed from 0.66 mm diameter orifices so that their diameters were comparable to the smallest amplifier dimension. For these orifices, the ratios $R_D/R_o = 7.0$ and $R_f/R_D = 11.4$, thus the orifices provide a nearly ideal pressure divider. With the feedback pressure $P_{fd} = 1/2\ P_{od}$, the feedback circuit should be stable as shown in the Nyquist plot of Figure 13.

The amplifier was set up in the configuration with the pressure divider as shown in the schematic and photograph of Figure 15. For this configuration, the static pressure gain for a single differential input to the summing amplifier with the second input grounded is simply a function of static resistances and from equation (4) can be calculated as 63. Test results run on the amplifier are shown in Figure 16. The data illustrate a linear gain of 60 with a null offset less than 5% of full scale value.

---

*Both the resistance and inertance increase linearly with length.

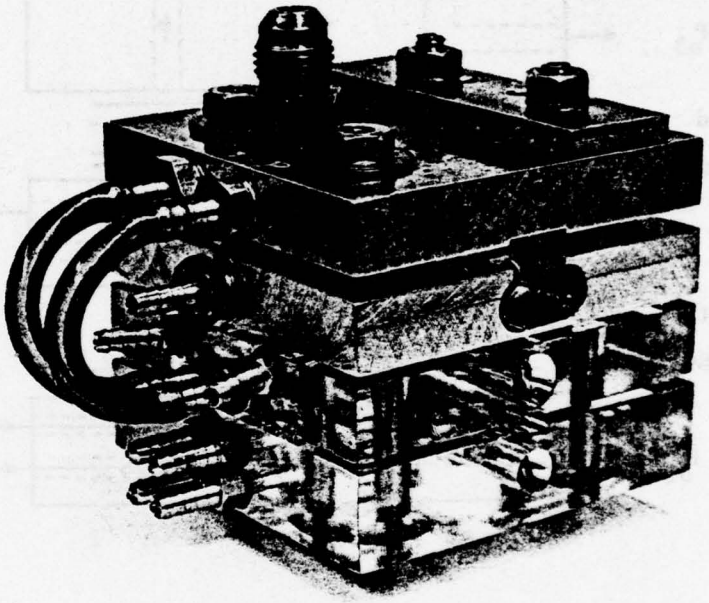

FIGURE 15a. PHOTOGRAPH OF SUMMING AMPLIFIER

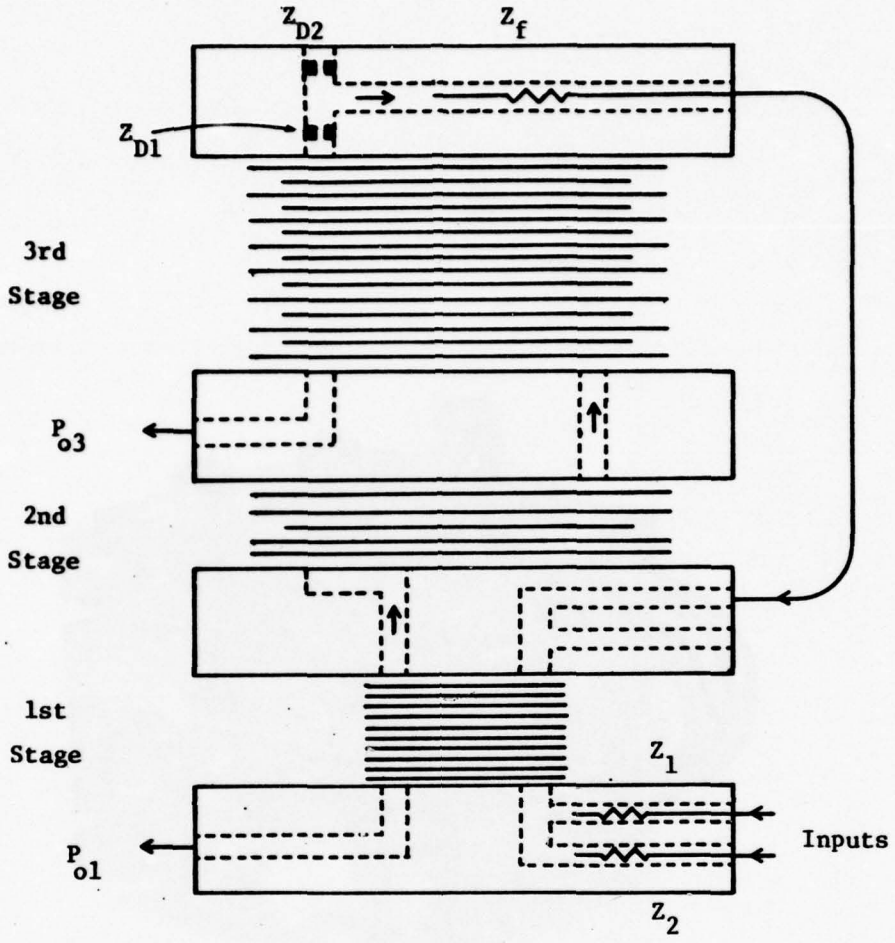

FIGURE 15b. SCHEMATIC OF SUMMING AMPLIFIER

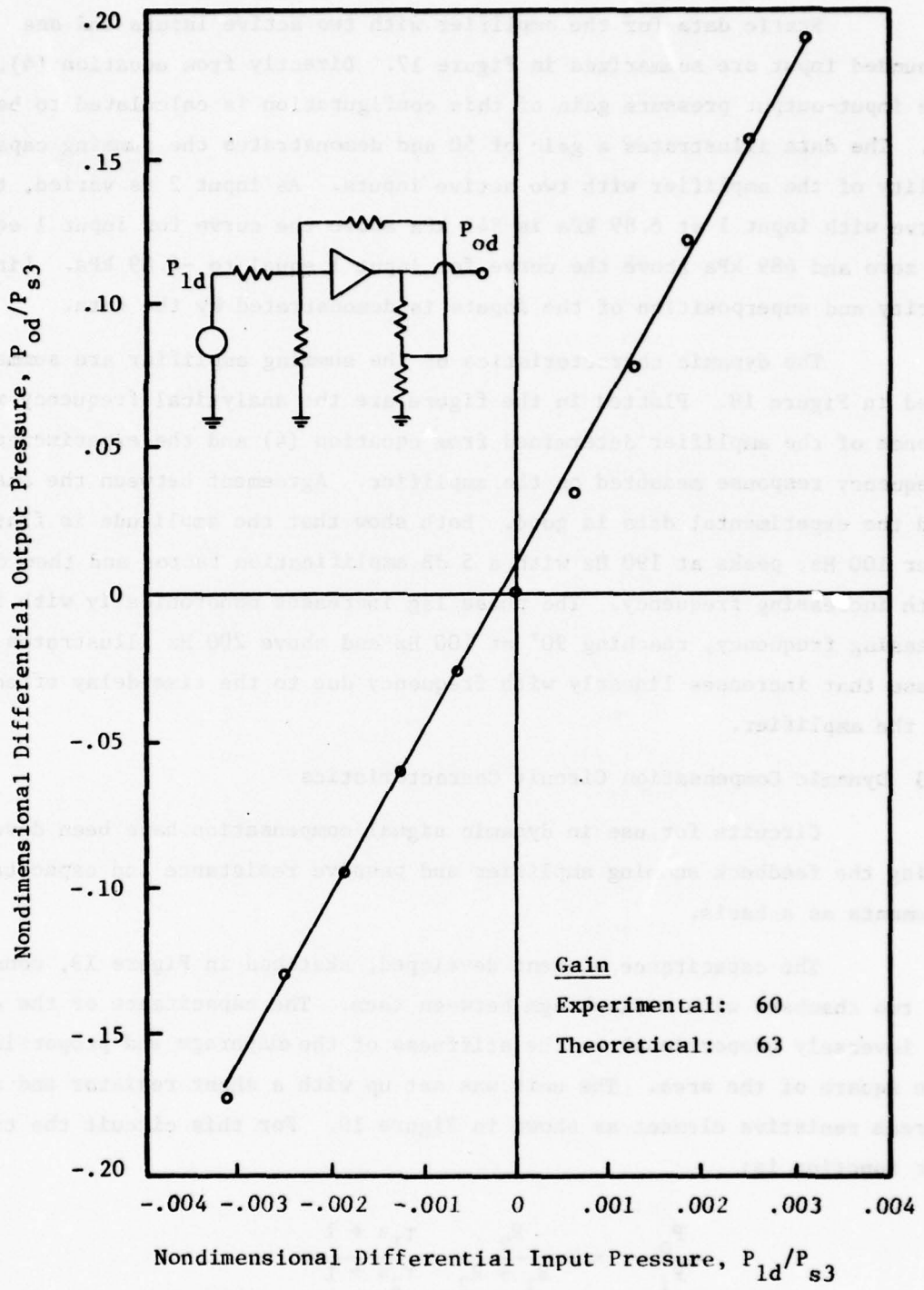

FIGURE 16. SUMMING AMPLIFIER SINGLE-INPUT STATIC GAIN CHARACTERISTICS

Static data for the amplifier with two active inputs and one grounded input are summarized in Figure 17. Directly from equation (4), the input-output pressure gain of this configuration is calculated to be 49. The data illustrates a gain of 50 and demonstrates the summing capability of the amplifier with two active inputs. As input 2 is varied, the curve with input 1 at 6.89 kPa is 345 kPa above the curve for input 1 equal to zero and 689 kPa above the curve for input 1 equal to -6.89 kPa. Linearity and superposition of the inputs is demonstrated by the data.

The dynamic characteristics of the summing amplifier are summarized in Figure 18. Plotted in the figure are the analytical frequency response of the amplifier determined from equation (4) and the experimental frequency response measured on the amplifier. Agreement between the analysis and the experimental data is good. Both show that the amplitude is flat to over 100 Hz, peaks at 190 Hz with a 5 dB amplification factor and then decreases with increasing frequency. The phase lag increases monotonically with increasing frequency, reaching 90° at 100 Hz and above 200 Hz illustrates a phase that increases linearly with frequency due to the time delay effects in the amplifier.

2.3 Dynamic Compensation Circuit Characteristics

Circuits for use in dynamic signal compensation have been developed using the feedback summing amplifier and passive resistance and capacitance elements as a basis.

The capacitance element developed, sketched in Figure 19, consists of two chambers with a diaphragm between them. The capacitance of the element is inversely proportional to the stiffness of the diaphragm and proportional to the square of the area. The unit was set up with a shunt resistor and a downstream resistive element as shown in Figure 19. For this circuit the transfer function is:

$$\frac{P_o}{P_i} = \frac{R_2}{R_1 + R_2} \frac{\tau_1 s + 1}{\tau_2 s + 1} \qquad (6)$$

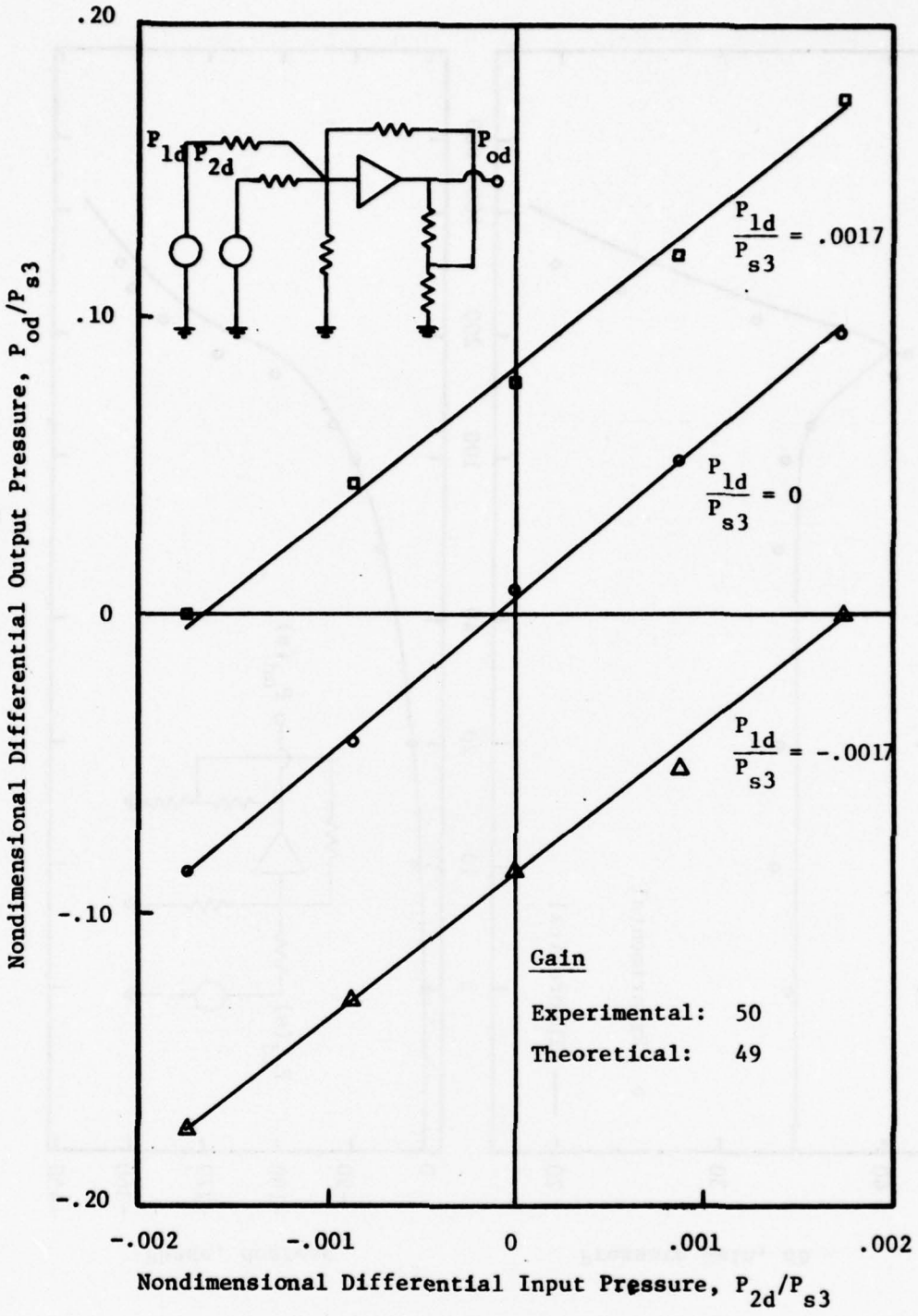

FIGURE 17. SUMMING AMPLIFIER MULTI-INPUT STATIC GAIN CHARACTERISTICS

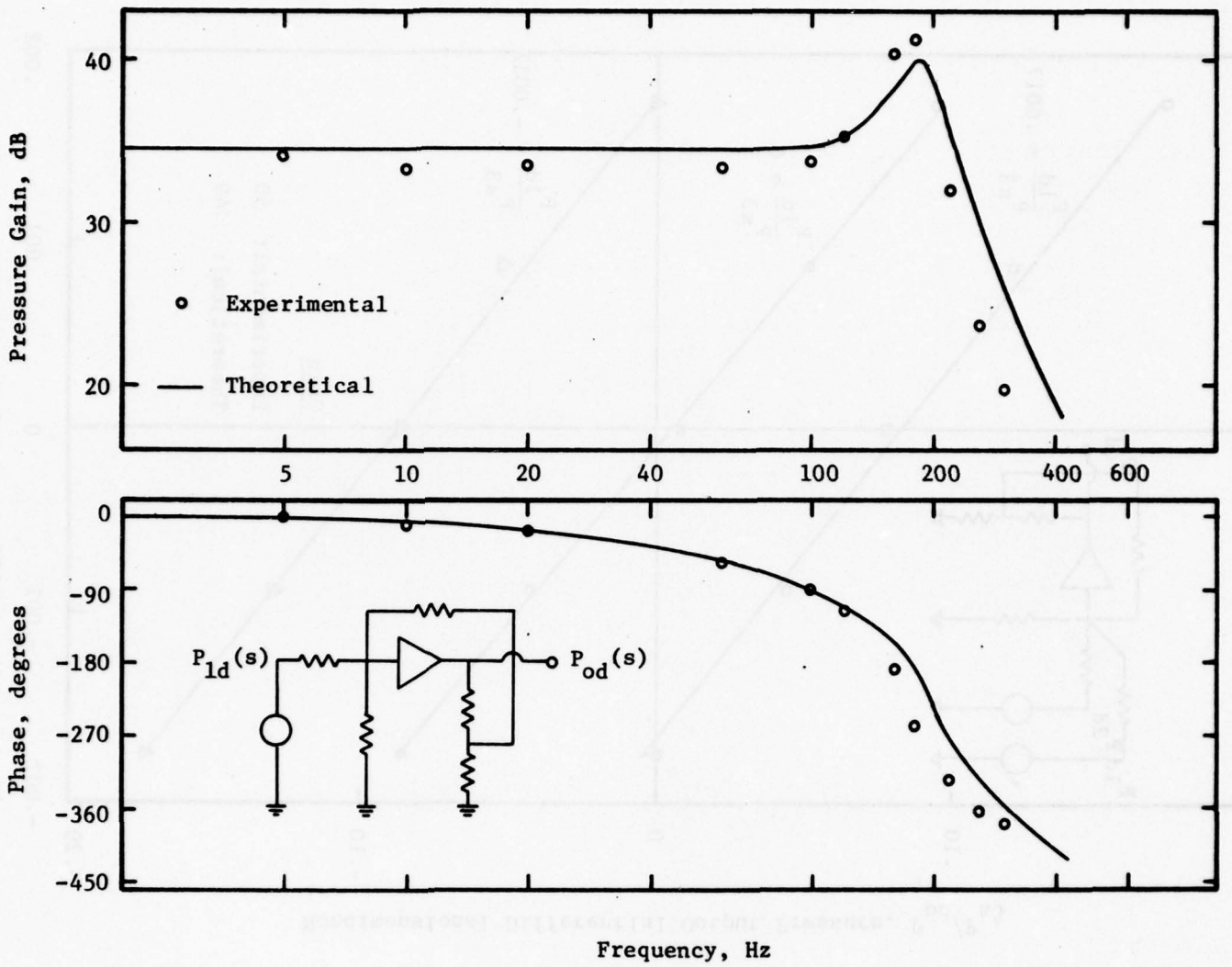

FIGURE 18. BLOCKED LOAD FREQUENCY RESPONSE OF SUMMING AMPLIFIER

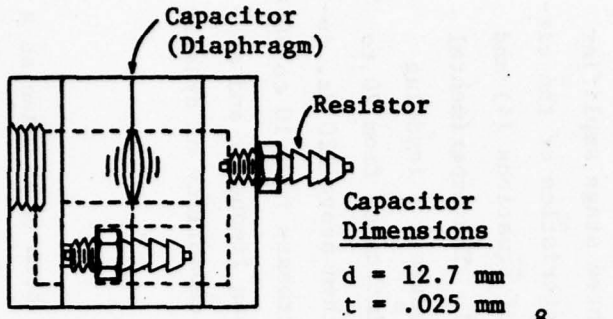

(a) Schematic of R-C Circuit

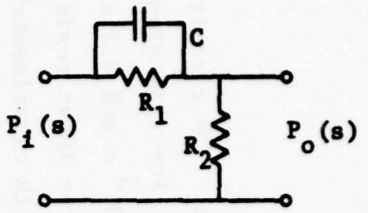

(b) R-C Circuit Diagram

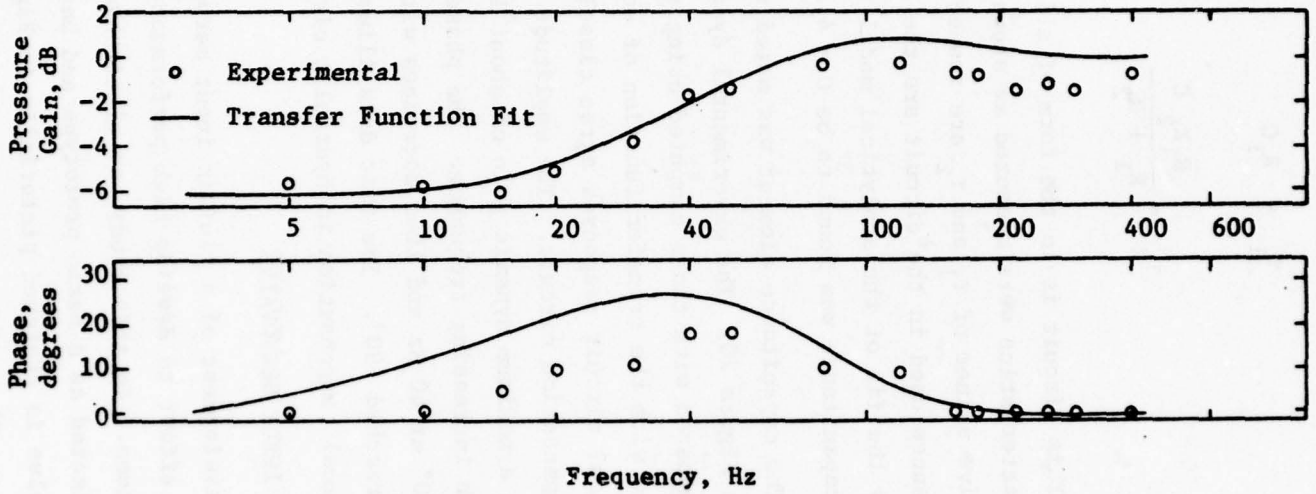

(c) Frequency Response

FIGURE 19. SKETCH AND DYNAMIC CHARACTERISTICS OF FLUID RESISTOR-CAPACITOR ELEMENT

where:

$$\tau_1 = R_1 C$$

$$\tau_2 = \frac{R_1 R_2 C}{R_1 + R_2}$$

This circuit is in the form of a lead-lag circuit. The circuit dynamic characteristics were measured as shown in Figure 19. For this element the effective values of τ_1 and τ_2 are respectively 6.4×10^{-3} s and 3.2×10^{-3} s. The resistances used in the circuit are the same value as the input resistors. As shown by the fit of the analytical model equation (6) with experimental data, the capacitance was found to be $C = 4.4 \times 10^{-13}$ m^5/N.*

The capacitance element was mated with the three stage amplifier as shown in Figure 20. The experimental dynamic characteristics of the circuit are compared with those computed using the model of equations (4) and (5) modified with the transfer function of equation (6). The experimental and analytical circuit responses agree closely and illustrate a lead-lag type of compensation circuit. The amplitude response increases from 20 to 100 Hz with a maximum dynamic gain of about 10 db and then above 120 Hz, decreases with increasing frequency. The phase shift increases from 10 to 40 Hz reaching +10° at 40 Hz and then decreases with increasing frequency and at 100 Hz has reached -90°. The test data illustrate the capability of dynamic lead-lag signal compensation in hydraulic circuits.

3. FLUIDIC INPUT SERVOVALVE

Development of a fluidic input servovalve has been undertaken as a part of the effort to develop high performance components for hydraulic actuation systems. In this study, an electrohydraulic two stage servovalve has been selected as a basic prototype and has been modified for fluidic input. The valve is sketched pictorially in Figure 21 with the fluidic input modifications. The valve is a Moog Model 50 x 451 servovalve** which has

---

*The capacitance was determined experimentally by the data of Figure 19, and equation (6), since computation of the effective diaphragm stiffness in its support structure could not be performed accurately.

**Although not shown in the schematic, the valve also has capability for direct mechanical input through an arm that moves a sleeve encompassing the spool. This mechanical input was not used in the tests described in this study.

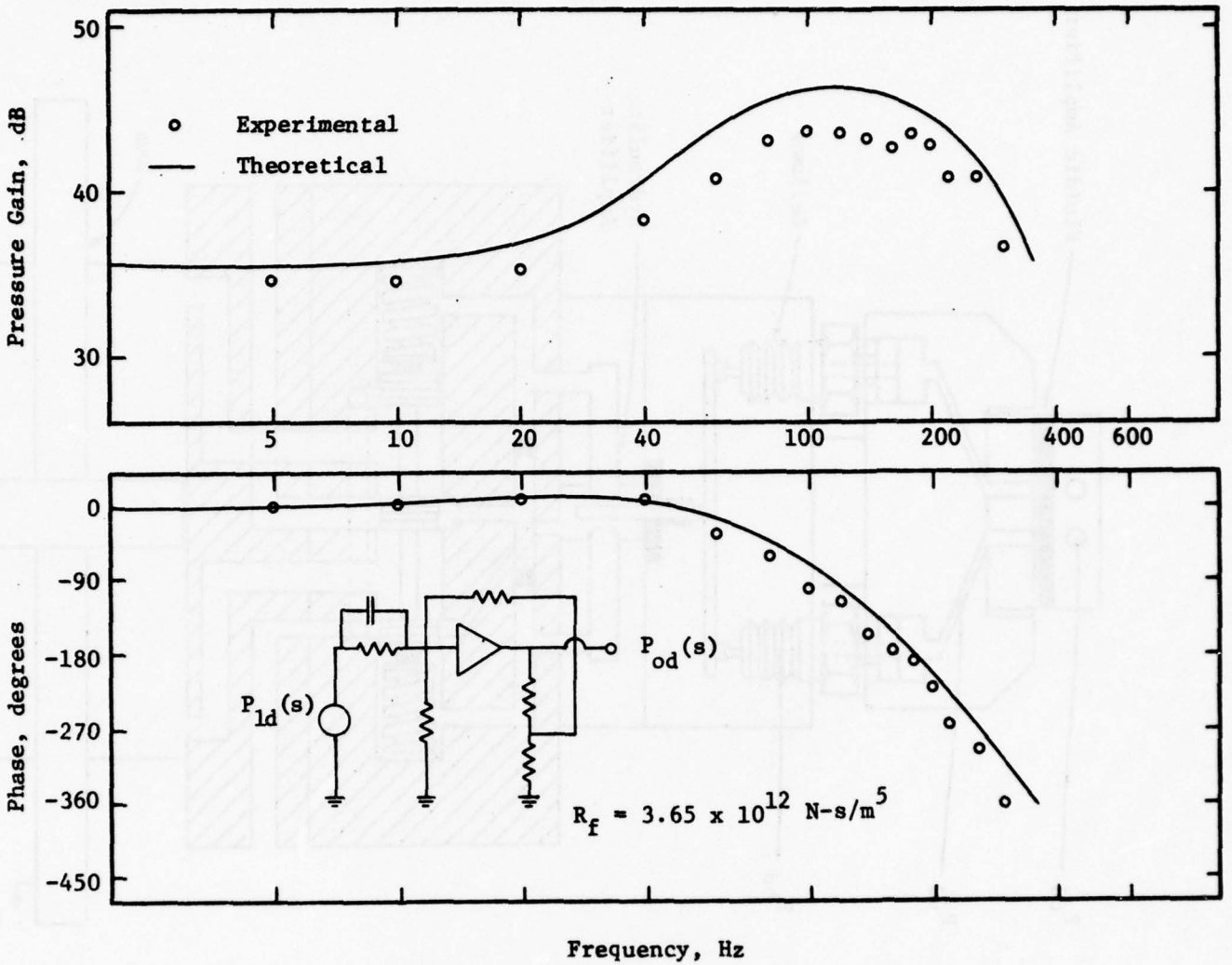

FIGURE 20. FREQUENCY RESPONSE CHARACTERISTICS OF DYNAMIC COMPENSATION CIRCUIT

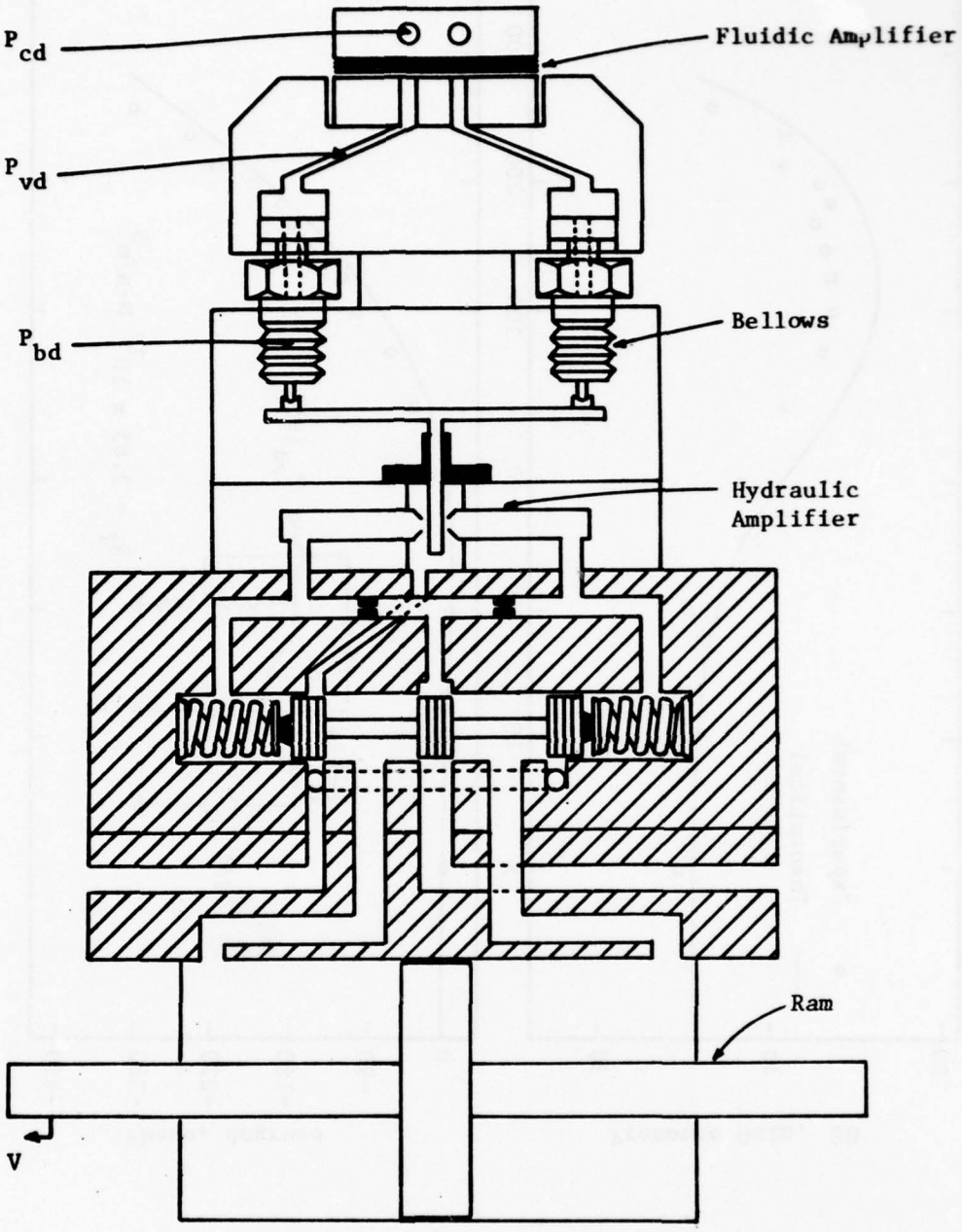

FIGURE 21. SCHEMATIC OF TWO STAGE SERVOVALVE

had the torque motor deactivated and has had bellows installed in order to position the first stage flapper. The valve consists of a pair of bellows which receive low pressure fluid inputs. The bellows provide a force differential on the flapper. The flapper controls the openings in the first stage flapper nozzle valve which in turn provides a pressure differential to the ends of the second stage spool. In the fluidic input valve the force balance involves the bellows forces and the flapper forces; thus, the only modification from the commercial version of the valve, is replacement of the torque motor forces on the flapper with the bellows forces. The commercial electrohydraulic valve characteristics and the bellows dimensions are summarized in Table II.

The valve with bellows installed was first tested statically. A differential pressure was applied to the bellows and then the pressure differential developed by the first stage flapper-nozzle across the spool ends and the flow from the second stage were measured with no load across the second stage output. The first stage pressure data is presented in Figure 22 while the second stage flow data is presented in Figure 23. The first stage differential pressure gain per unit differential bellows pressure data illustrates good linearity with a differential gain of 44. The second stage output flow per unit differential bellows pressure data is linear with a gain of 5.0×10^{-10} $m^5/N\text{-}s$.

To provide the servovalve with low level fluidic input capability of 7 kPa, a fluid amplifier input stage was designed to drive the bellows assembly. The design of the fluid amplifier was based upon a single stage amplifier consisting of 231004A laminates. The design goals for the amplifier were to provide a pressure gain greater than 5, with input levels of 0-7 kPa so that the bellows can be driven to its full range. Also a primary consideration in the design is dynamic performance. It is desired to have the fluidically driven valve dynamic performance be comparable to that of the electrohydraulic commercial valve. A single stage amplifier section was constructed with characteristics as summarized in Table III. This section is similar to the first stage amplifier of the three stage gain block and thus could be expected to provide the static gain characteristics desired. To prevent dynamic loading of the amplifier due to the bellows capacitance-amplifier output impedance, the time constant associated with the bellows

TABLE II. SERVOVALVE BELLOWS PARAMETERS

Control Pressure Ratings	Rated	Proof
Differential Input	34.5 kPa (5 psid)	68.9 kPa (10 psid)
Input High Side, with Respect to Return		276 kPa (40 psid)
Inputs and Return, in Common		689.5 kPa (100 psig)

Servovalve Pressure Rating	Rated	Proof
Supply	1.0×10^4 kPa (1500 psi)	2.06×10^4 kPa (3000 psi)
Supply and Return in Common		1.0×10^4 kPa (1500 psi)

Bellows Effective Area	31.9 mm^2 (.0495 in^2)

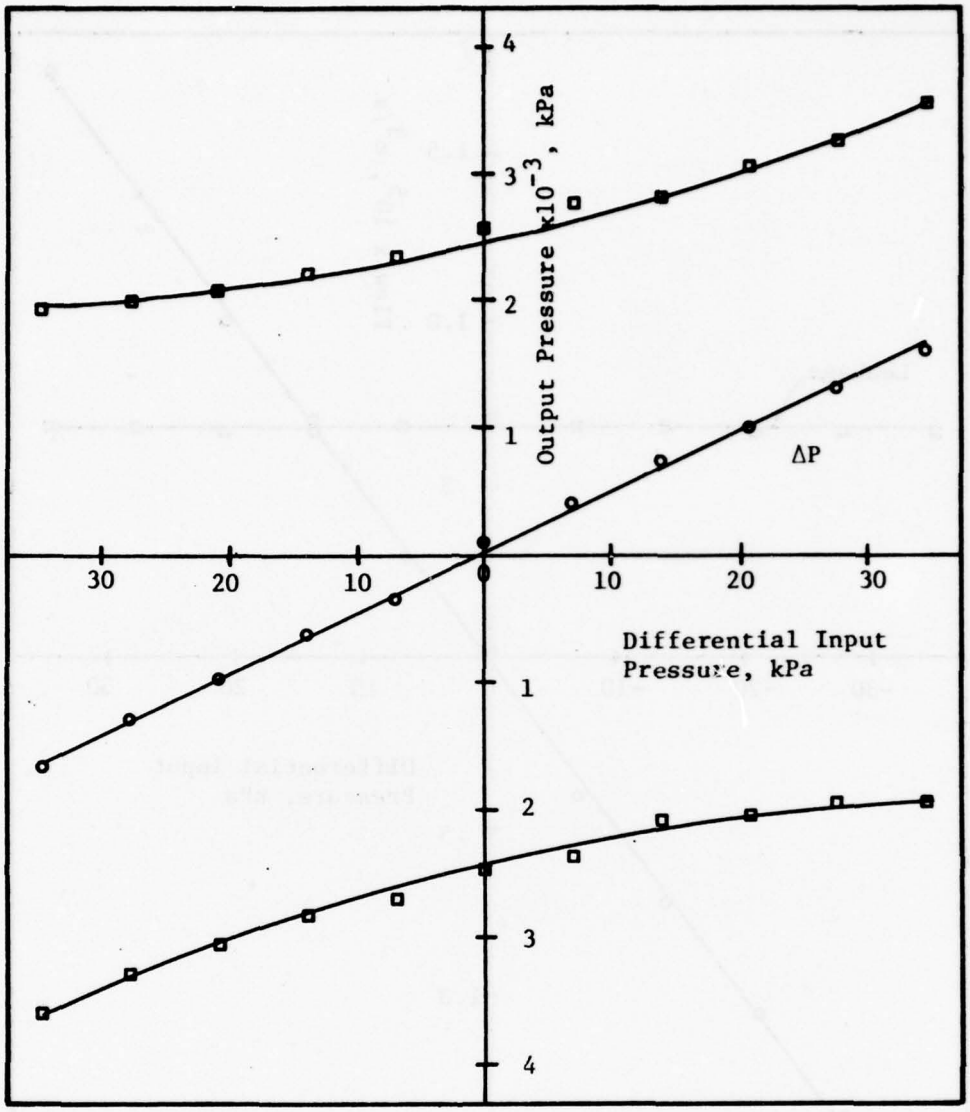

FIGURE 22. VALVE FIRST STAGE PRESSURE GAIN

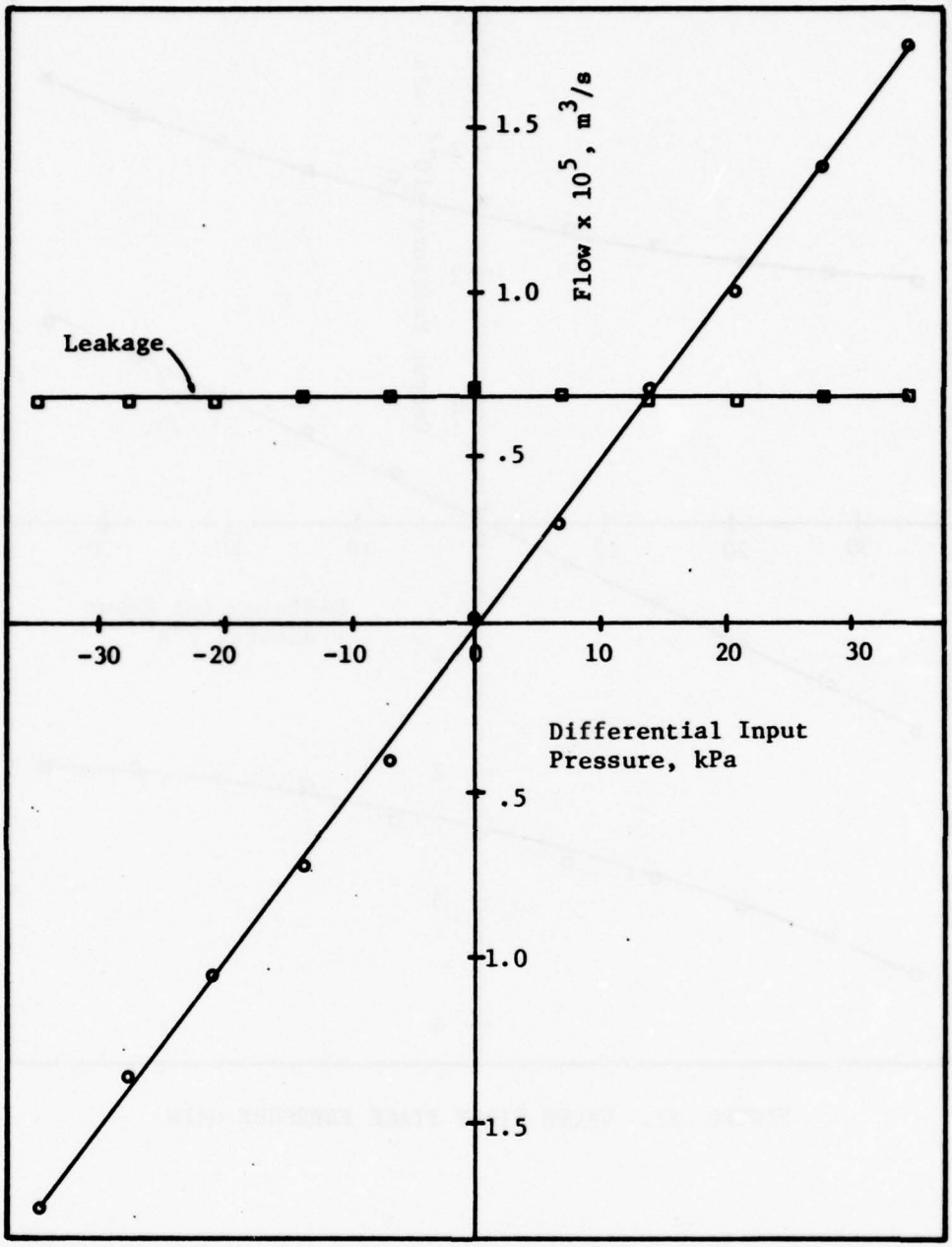

FIGURE 23. VALVE FLOW VERSUS INPUT TO BELLOWS

TABLE III. SINGLE STAGE AMPLIFIER PARAMETERS

Laminate Design	231004A
Size, b_s (mm)	0.5
Aspect Ratio, σ	2
Supply Pressure, P_s (kPa) [psi]	110 [16]
Nondimensional Bias Pressure, P_{co}/P_s	.05
Static Pressure Gain	7

TABLE IV. RAM CHARACTERISTICS

Effective Piston Area	435. mm^2
Piston Mass	.078 kg

capacitance - amplifier output impedance was reduced by using two sections in parallel, thus cutting the output impedance by a factor of two. In exploratory dynamic testing, when only one section was used, distortion occurred in the bellows pressure signal.

The complete fluid amplifier-valve assembly was tested first statically and then dynamically. The static test data are summarized in Figure 24 and 25 as first stage flapper-nozzle valve output pressure versus fluid amplifier input pressure and as second stage valve output flow under no load versus fluid amplifier input pressure. Both sets of data show a good degree of linearity. The first stage pressure gain with respect to the fluid amplifier input is 320 and at a fluid amplifier input pressure of 6 kPa the full bellows pressure is achieved. The valve output flow to the fluid amplifier input pressure gain is 3.3×10^{-9} $m^5/N\text{-}s$. Thus the static data demonstrate that with input pressures in the range of 0 to 7 kPa, full valve operation may be achieved.

Dynamic data were taken with the valve output connected to a small hydraulic ram. The ram characteristics are summarized in Table IV. With this light weight ram, the ram velocity is a measure of the valve flow under no load conditions. Tests were run by introducing a sinsuoidally varying pressure signal at the fluid amplifier input and then measuring this input pressure, the pressure at the bellows and the ram velocity. The pressures were measured with piezoelectric pressure transducers while the ram velocity was measured with a LVSYN velocity transducer. The response data are presented in Figure 26 as $\Delta P_{vd}/\Delta P_{cd}$ (valve differential pressure/input differential pressure) versus frequency and $\Delta V/\Delta P_{vd}$ (ram velocity/valve differential pressure) versus frequency and $\Delta V/\Delta P_{cd}$ the total system response. These three responses were measured independently and the summation of the amplifier and valve responses to equal the total response is a check on the experimental method. The amplitude response data show that the fluid amplifier increasing gain with frequency characteristic in the 0 to 130 Hz range combines with the decreasing gain of the valve to provide an overall amplitude that has decreased to 70% of its static gain at 30 Hz with the major reduction in gain due to the first and second stages of the valve. The phase characteristics show that at 30 Hz the

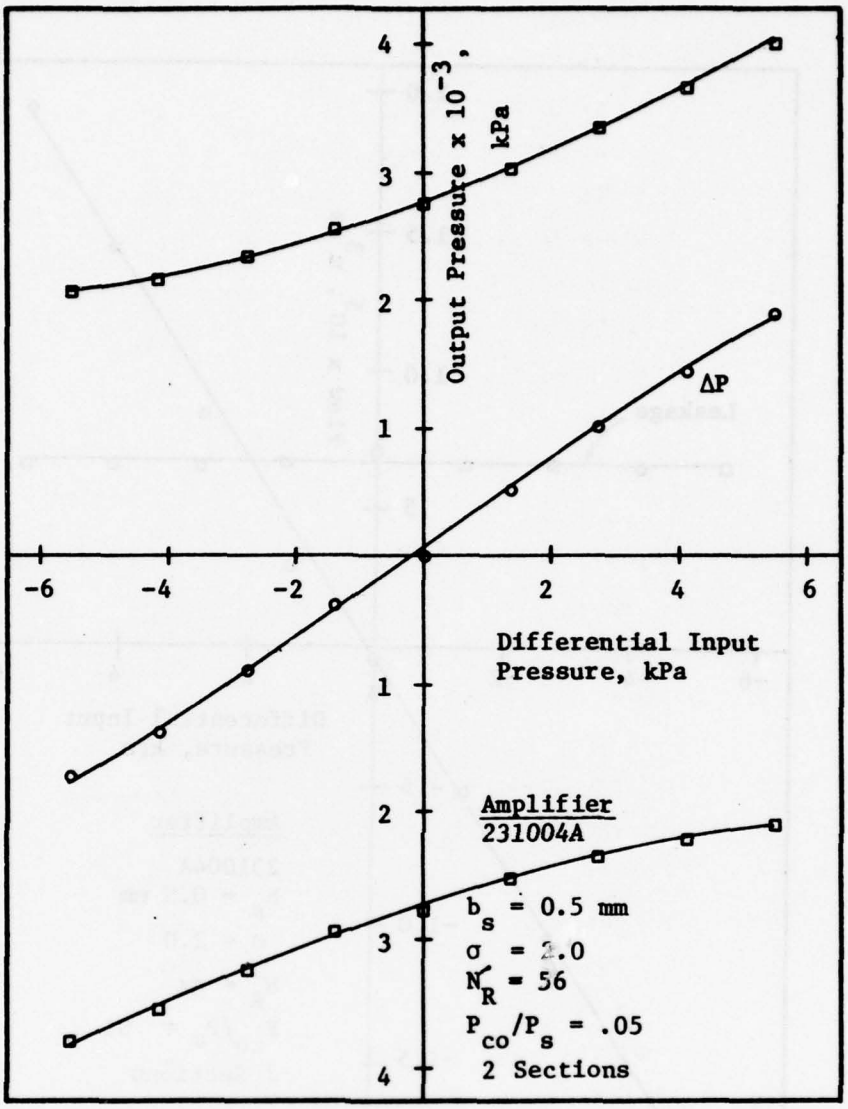

FIGURE 24. FLUIDIC INPUT VALVE PRESSURE GAIN

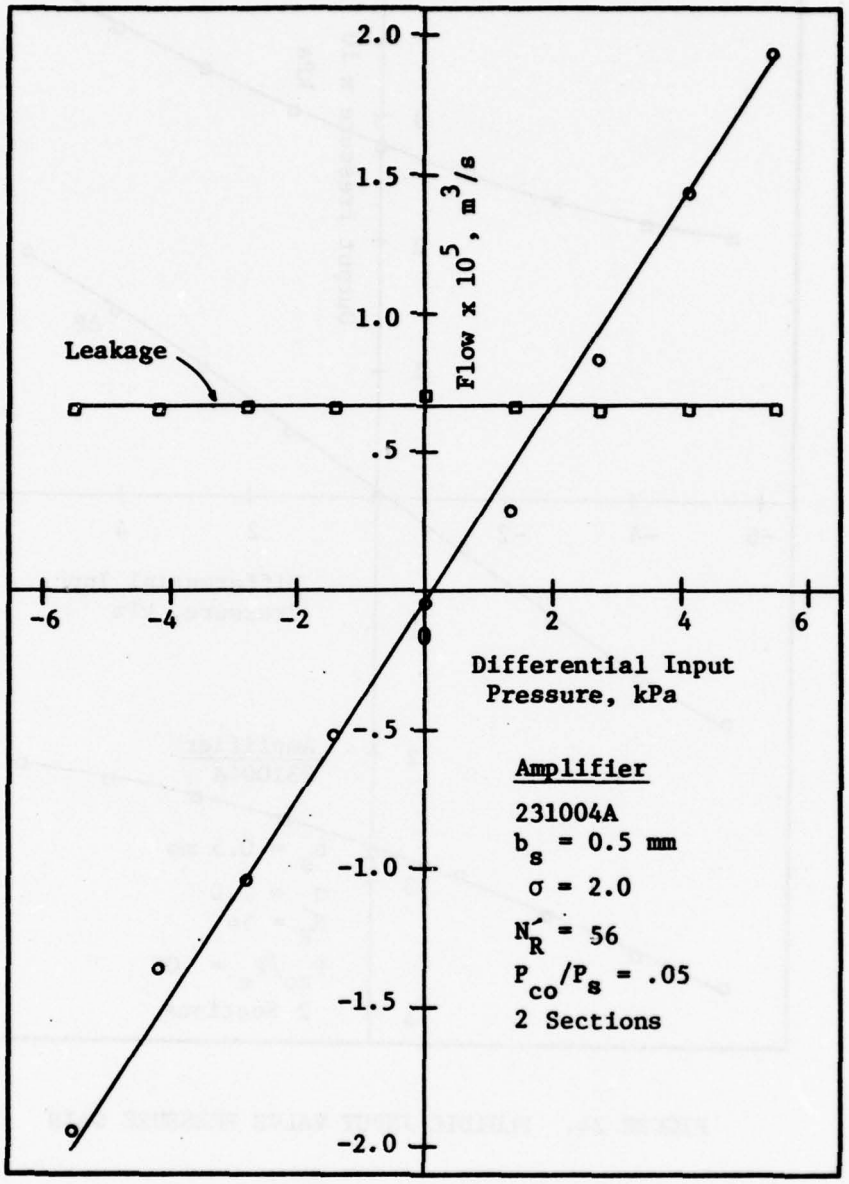

FIGURE 25. FLUIDIC INPUT VALVE FLOW VERSUS AMPLIFIER INPUT

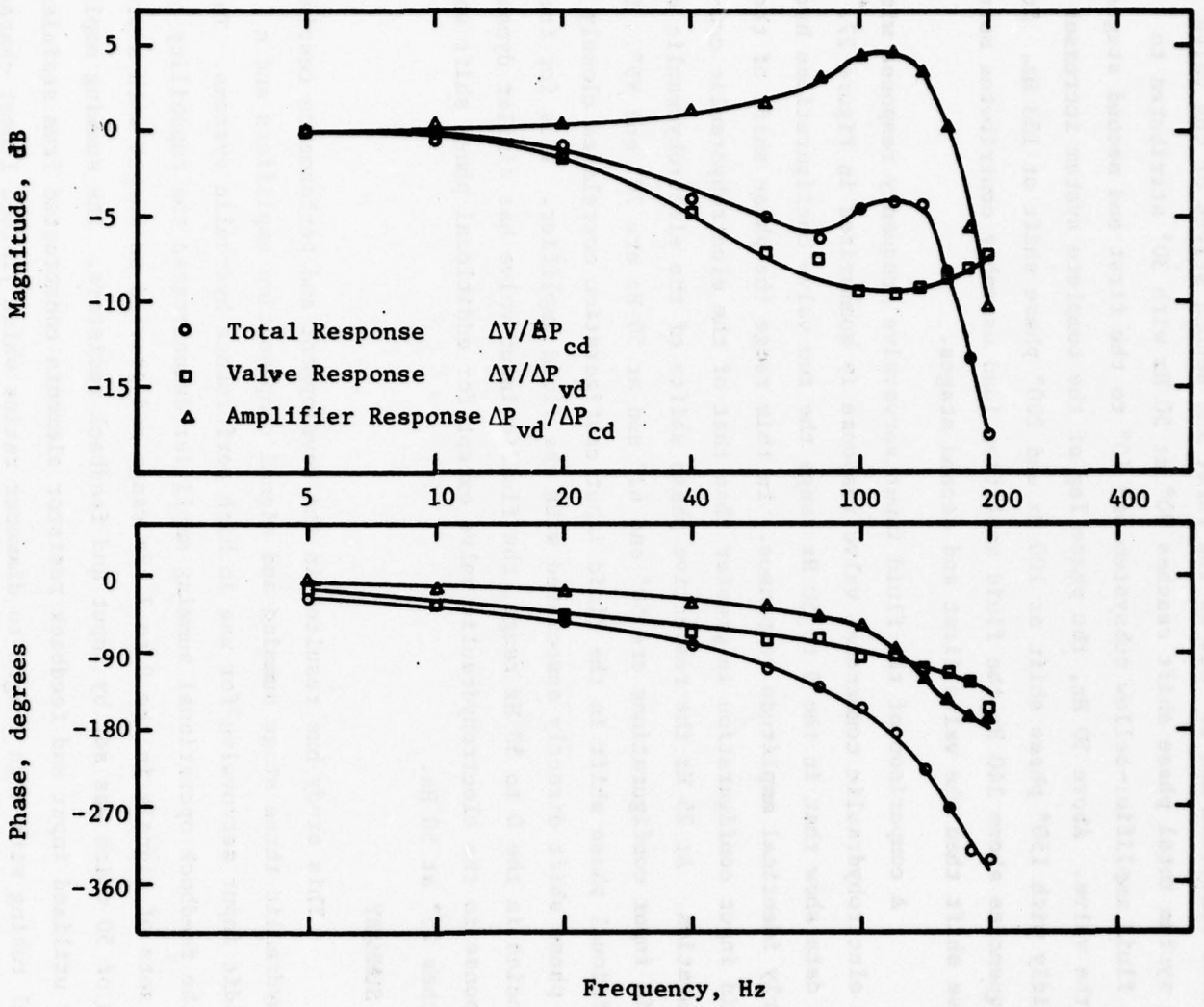

FIGURE 26. FLUIDIC INPUT VALVE FREQUENCY RESPONSE

total phase shift is 70° with 20° degrees attributed to the fluid amplifier-bellows subsystem and 50° due to the first and second stages of the valve. The system total phase shift reaches 90° at 50 Hz with 30° attributed to the fluid amplifier-bellow subsystem and 60° to the first and second stages of the valve. Above 50 Hz, the phase lag of the complete system increases rapidly with 150° phase shift at 100 Hz and 200° phase shift at 150 Hz. For frequencies above 140 Hz the fluid amplifier load assembly contributes more phase shift than the valve first and second stages.

A comparison of the fluid input servovalve frequency response with the electrohydraulic commercial valve response is summarized in Figure 27.* The data show that in the 0 to 50 Hz range the two valve configurations have nearly identical amplitude responses. In this range the phase shift of the fluid input configuration is greater than that of the electrohydraulic configuration. At 25 Hz the respective phase shifts of the electrohydraulic and fluid input configurations are 50° and 62° and at 50 Hz are 70° and 95°. The additional phase shift in the fluid input configuration correlates closely with the phase shift directly associated with the fluid amplifier. Thus for frequencies in the 0 to 50 Hz range, the fluidic input valve has similar dynamic response to the electrohydraulic valve except for additional phase shift which reaches 25° at 50 Hz.

4. SUMMARY

This study has resulted in the development and performance testing of hydraulic three stage summing and signal compensation amplifiers and a fluidic input servovalve for use in high performance hydraulic systems. Tests of the feedback operational summing amplifier demonstrated the capability to sum sets of signals in the 0 to 7 kPa range and provide an output with a pressure gain of 50 which was set by input and feedback resistors. The summing amplifier utilized input and feedback resistor elements constructed from stainless steel tubing with high length to diameter ratios which yielded linear characteristics over the operating range of interest. Tests conducted on the amplifier demonstrated both input-output linearity and superposition of inputs.

---

*The electrohydraulic valve response with the torque motor input was measured using a piston for flow measurement in a similar manner to that described above. The response was measured by Moog Valve Company.

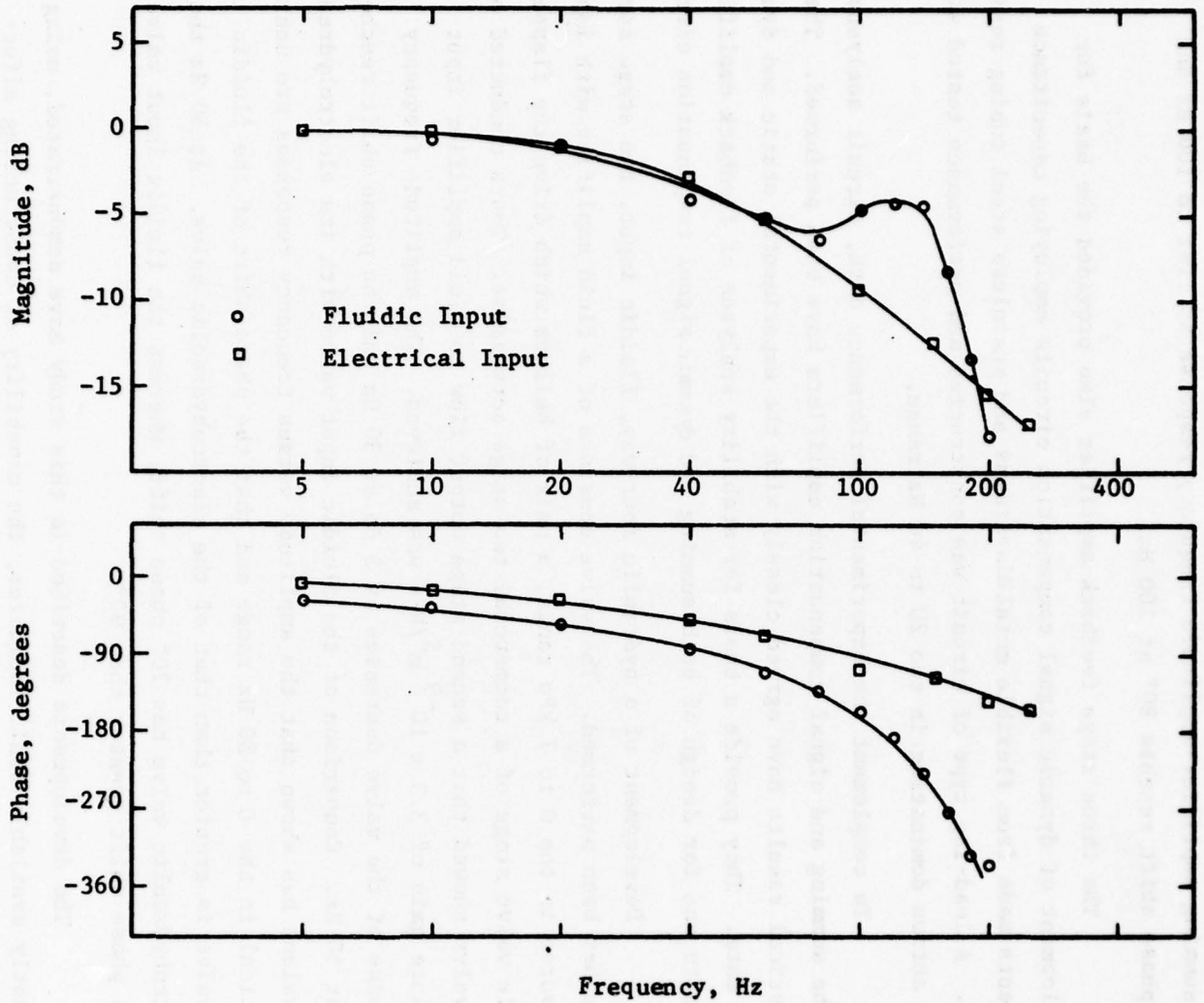

FIGURE 27. COMPARISON OF FLUIDIC AND ELECTROHYDRAULIC VALVE RESPONSES

The summing amplifier amplitude frequency response is flat to 100 Hz and the phase shift reaches 90° at 100 Hz.

The three stage feedback amplifier also provided the basis for development of dynamic signal compensation circuits employing capacitance elements made from flexible metal diaphragms and stainless steel tubing resistors. A lead-lag type of circuit was constructed and performance tested with lead action dominating in the 20 to 40 Hz range.

To complement the experimental performance data, circuit analyses of the summing and signal compensation amplifiers have been performed. These analytical results have agreed closely with the experimental static and dynamic test data. They provide a basis for stability analyses of feedback amplifier circuits and for design of both summing and dynamic signal compensation circuits.

Development of a hydraulic four-way, fluidic input, two stage servovalve has been performed. The valve consists of a fluid amplifier with input pressures in the 0 to 7 kPa range, a pair of bellows which drive the flapper-nozzle valve stage of a commercial two stage servovalve. Tests conducted on the valve showed that a second stage output flow to fluid amplifier input pressure gain of 3.3×10^{-9} $m^5/N\text{-}s$ was achieved. The amplitude frequency response of the valve decreases by 3 db at 30 Hz and the phase shift reaches 90° at 50 Hz. Comparison of the fluidic input valve with its electrohydraulic equivalent has shown that the amplitude versus frequency responses are nearly identical in the 0 to 50 Hz range and that the phase shift of the fluidic input valve is greater than that of the electrohydraulic valve. At 50 Hz the electrohydraulic valve has 70° phase shift, whereas the fluidic input valve has a phase shift greater than 90°.

The developments described in this study have demonstrated, using currently available fluid laminates, the capability of constructing effective summing and signal compensation elements in a hydraulic medium. These elements, with the fluid input servovalve provide a capability to construct closed-loop, high power level hydraulic systems in which sensing, signal compensation and power level modulation functions are performed with hydromechanical components.

The research described in this report completes the second phase of work directed to high performance hydraulic system development. Work in the next phases of research will focus upon integration of components into a complete system and upon the problems associated with operation of hydraulic systems over wide ranges in temperature.

APPENDIX A. DRAWINGS OF LAMINATE DESIGN

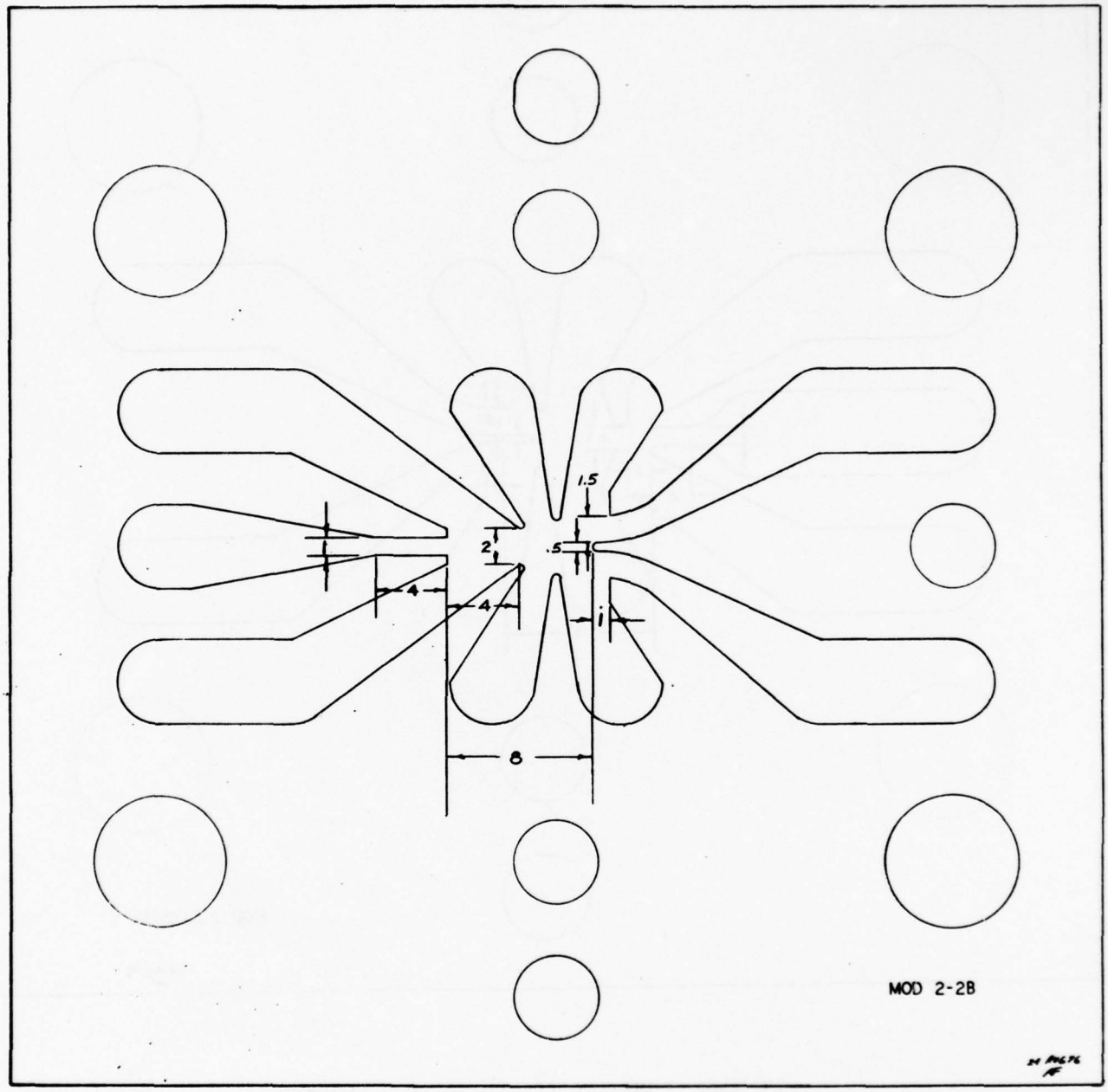

2-2B LAMINATE SCALED IN NOZZLEWIDTHS

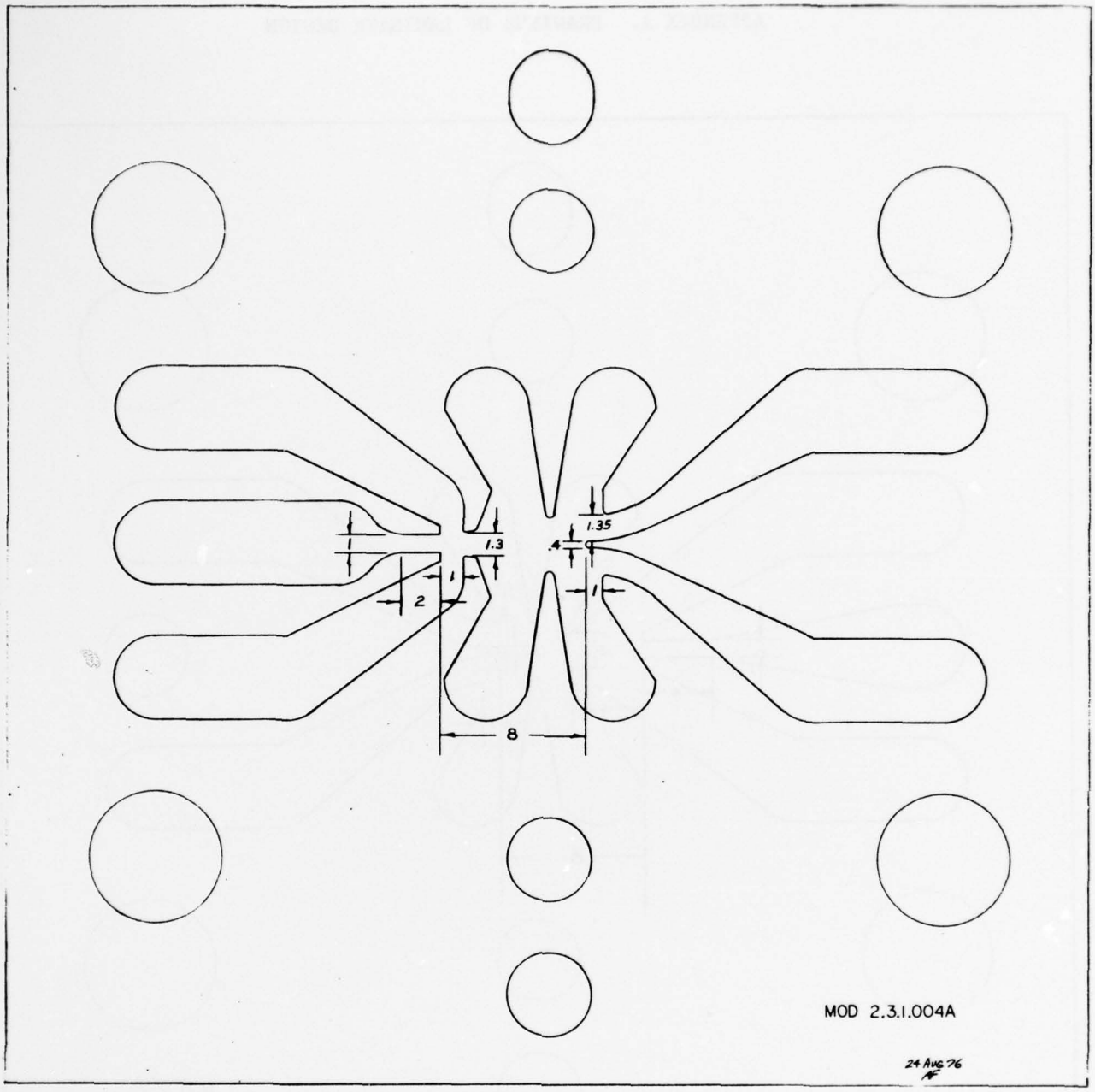

231004A LAMINATE SCALED IN NOZZLEWIDTHS

NOMENCLATURE

A_i	tube area of resistor i (mm^2)
b_s	supply nozzle width (mm)
C	capacitance (m^5/N)
d_i	tube diameter of resistor i (mm)
h	laminate thickness (mm)
I_i	inertance of resistor i ($N\text{-}s^2/m^5$)
K	static gain
ℓ_i	tube length of resistor i (mm)
N_R	Reynolds number
N_R'	modified Reynolds number
P_{bd}	bellows pressure differential (kPa)
P_c	control port pressure (kPa)
P_{cd}	control port pressure differential (kPa)
P_{co}	control port pressure bias $((P_{cl\ell} + P_{clr})/2)$ kPa
P_{fd}	feedback pressure differential (kPa)
P_i	input pressure (kPa)
P_o	output port pressure, output pressure (kPa)
P_{od}	output port pressure differential (kPa)
P_{vd}	valve input pressure differential (kPa)
P_s	supply pressure (kPa)
P_1, P_2	summing amplifier input pressure (kPa)
P_{1d}, P_{2d}	summing amplifier input pressure differential (kPa)
Q_c	control port flow (m^3/s)
Q_o	output port flow (m^3/s)
Q_s	power jet supply flow (m^3/s)
R	resistance ($N\text{-}s/m^5$)
R_D, R_{D1}, R_{D2}	pressure divider resistance ($N\text{-}s/m^5$)
R_f	feedback resistance ($N\text{-}s/m^5$)
R_g	grounding resistance ($N\text{-}s/m^5$)
R_i	resistance of resistor i ($N\text{-}s/m^5$)
R_o	amplifier output resistance ($N\text{-}s/m^5$)
R_1, R_2	resistors ($N\text{-}s/m^5$)

R^*, R^{**}	resistance as defined in eq. (4)
s	Laplace transform operator
T	output-input pressure transfer function
T_1	first order lag time constant (s)
V	ram velocity (m/s)
x_{th}	supply nozzle throat length (mm)
Z_a	amplifier input impedance ($N\text{-}s/m^5$)
Z_{D1}, Z_{D2}	pressure divider impedance ($N\text{-}s/m^5$)
Z_f	feedback resistor impedance ($N\text{-}s/m^5$)
Z_g	grounding resistor impedance ($N\text{-}s/m^5$)
Z_i	impedance of resistor i ($N\text{-}s/m^5$)
Z_o	output impedance ($N\text{-}s/m^5$)
Z_1, Z_2	input resistor impedance ($N\text{-}s/m^5$)
$\Delta( )$	increment or difference of a quantity ( )
μ	absolute viscosity
ξ	second order factor damping ratio
ρ	fluid density (kg/m^3)
σ	amplifier power nozzle aspect ratio [h/b_s]
τ	delay time constant (s)
τ_i	time constant of resistor i (s)
τ_1, τ_2	time constants (s)
ω_n	second order factor natural frequency (rad/s)

SUBSCRIPTS

ℓ	left
r	right
1	first stage
2	second stage
3	third stage

Fluidics Distribution List

Commander IDDR & E
Pentagon, Room 3D 1089
Washington, DC 20310
ATTN: Dr. David A. Charvonia

Defense Documentation Center
Cameron Station, Building 5
Alexandria, VA 22314
ATTN: DDC-TCA 22314
ATTN: DDC-TCA 12 copies

Office of the Deputy Chief of Staff for
Research, Development & Acquisition
Department of the Army
Washington, DC 20310
ATTN: DAMA-ARP-P, Dr. V. Garber
ATTN: Major P. Tate, Rm 3D424

US Army R&D Group (Europe)
Box 15
FPO, NY 09510
ATTN: Chief, Aeronautics Branch
ATTN: Chief, Engineering Sciences

US Army Research Office
P. O. Box 12211
Research Triangle Park, NC 27709
ATTN: James J. Murray, Eng Sci Div

Commander
USA Foreign Science & Technology Center
Federal Office Building
220 7th Street NE
Charlottesville, VA 22901
ATTN: AMXST-IS3, C. R. Moore

Director
Eustis Directorate
USA Air Mobility Res & Dev Lab
Fort Eustis, VA 23604
ATTN: SAVDL-EU-SYA, George W. Fosdick

Commander
USA Missile Command
Redstone Arsenal, AL 35809
ATTN: Redstone Scientific Information Center, AMSMI-RBD
ATTN: AMSMI-RGC, William Griffith
ATTN: AMSMI-RGC, James G. Williams
ATTN: AMSMI-RGC, J. C. Dunaway
ATTN: AMCPM-TOE, (Fred J. Cheplen)

Commander
USA Mobility Equipment R&D Center
Fort Belvoir, VA 22060
ATTN: Technical Library (Vault)
ATTN: DRXFB-EM, R. N. Ware

Commander
Edgewood Arsenal
Aberdeen Proving Ground, MD 21010
ATTN: SAREA-MT-T (Mr. D. Patton)

Commander
Picatinny Arsenal
Dover, NJ 07801
ATTN: SARPA-ND-C-C (D. Sampar)
ATTN: SARPA-TS-S-#59
ATTN: SARPA-ND-C-C (A. E. Schmidlin)

Commander
Watervliet Arsenal
Watervliet Arsenal, NY 12189
ATTN: Gary W. Woods
ATTN: SARWV-RDT-L
ATTN: John Barrett

Commander
USA Tank Automotive Command
Armor & Comp Div, DRDTA-RKT
Building 215
Warren, MI 48090
ATTN: T. Kozowyk
ATTN: M. Steele

Commander
White Sands Missile Range, NM 88002
ATTN: STEWS-AD-L, Technical Library

Commander
US Army Armament Command
Rock Island, IL
ATTN: AMSAR-RDG-T (Mr. R. Spencer)
ATTN: AMSAR-ASF

Commander
Rodman Laboratories
Rock Island Arsenal
Rock Island, IL 61201
ATTN: SARRI-LA

BMD Advanced Technology Center
P. O. Box 1500
Huntsville, AL 35807
ATTN: J. Papadopoulos

Office of Naval Research
Department of the Navy
Arlington, VA 22217
ATTN: Stanley W. Doroff, Code 438
ATTN: D. S. Siegel, Code 211

Commander
Naval Air Development Center
Warminster, PA 18974
ATTN: Ed. Schmidt (30424)
ATTN: Code 8134, Lois Guise

Commanding Officer
Naval Air Engineering Center
Lakehurst, NY 08733
ATTN: ESSD, Code 9314, Harold Ott

Naval Air Systems Command
Code: Air-52022A (J. Burns)
Dept of the Navy
Washington, DC 20360

Commander
Pacific Missile Range
Naval Missile Center
Point Mugu, CA 93042
ATTN: Abe J. Garrett, Code 4121.2
ATTN: Code 1230, A. Anderson

Commander
Naval Ship Engineering Center
Philadelphia Division
Philadelphia, PA 19112
ATTN: Code 6772, D. Keyser

Commander
Naval Surface Weapons Center
White Oak, MD 20910
ATTN: Clayton McKindra, Code 413
ATTN: Code WA-33, J. O'Steen

Naval Postgraduate School
Mechanical Engineering Dept
Monterey, CA 93940
ATTN: Prof. T. Sarpkaya

Commander
Naval Ordnance Station
Indianhead, MD 20640
ATTN: Code 5123B, J. Morris

Naval Ship Res & Dev Center
Code 5641
Bethesda, MD 20084

Naval Sea Systems Command
SEA0331H
Washington, DC 20362
ATTN: A. Chaikin

Commander
Naval Weapons Center
China Lake, CA 93555
ATTN: Code 533, Library Division

Commander
AF Aero Propulsion Laboratory, AFSC
Wright-Patterson AFB, OH 45433
ATTN: Lester Small ITBC

Commander
Air Force Avionics Lab
Wright-Patterson AFB, OH 45433
ATTN: RWN-2 (Richard Jacobs)

Director
AF Office of Scientific Research
1400 Wilson Blvd
Arlington, VA 22209
ATTN: NE (Mr. George Knausenberger)

Commander
Air Force Flight Dynamics Laboratory
ATTN: AFFDL/FGL (H. Snowball)
Wright-Patterson AFB, OH 45433

Commander
AF Weapons Laboratory, AFSC
Kirtland AFB, NM 87117
ATTN: SUL, Technical Library

Commander
Armament Development & Test Center
Eglin Air Force Base, FL 32542
ATTN: ADTC (DLOSL), Tech Library

Air Force Flight Test Center
6510 ABG/SSD
Edwards AFB, CA 93523
ATTN: Technical Library

4950th Test Wing (TZHM)
Wright-Patterson AFB, OH 45424
ATTN: Mr. Michael Collins

AF Institute of Technology, AU
Wright-Patterson AFB, OH 45433
ATTN: Library AFIT (LD), Bldg. 640, Area B
ATTN: AFIT (ENM), Milton E. Franke (3 copies)

Aerospace Medical Division
ATTN: AMD/RDN, Cpt. G. James
Brooks AFB, TX 78235

Div of Reactor Research & Development
F-309 USERDA
Washington, DC 20545
ATTN: Frank C. Legler

Oak Ridge National Laboratory
Central Res Library, Bldg. 4500N, Rm. 175
P. O. Box X
Oak Ridge, TN 37830
ATTN: E. Howard

Department of Commerce
Bureau of East-West Trade
Office of Export Administration
Washington, DC 20230
ATTN: Walter J. Rusnack

Scientific Library
US Patent Office
Washington, DC 20231
ATTN: Mrs. Cureton

Department of Commerce
National Bureau of Standards
Washington, DC 20234
ATTN: Gustave Shapiro, 425.00

NASA Ames Research Center
Moffett Field, CA 94035
ATTN: MS 244-13, Dean Chisel

NASA Langley Research Center
Hampton, VA 23665
ATTN: H. D. Garner, MS 494
ATTN: R. R. Hellbaum, MS 494
ATTN: MS 185, Technical Library

NASA Lewis Research Center
21000 Brookpark Road
Cleveland, OH 44135
ATTN: Vernon D. Gebben

NASA Scientific & Tech Info Facility
P. O. Box 8657
Baltimore/Washington International Airport, MD 21240
ATTN: Acquisitions Branch

National Heart & Lung Inst.
Division of Lung Diseases
Bldg. WW, Rm. 6A03
Bethesda, MD 20014
ATTN: Dr. P. J. Zalesky

Dept of HEW
Public Health Service
National Inst. of Health
Bldg. 13, Rm. 3W-13
Bethesda, MD 20014
ATTN: C. J. McCarthy

University of Alabama
Civil & Mineral Engineering Dept
P. O. Box 1468
University, AL 35486
ATTN: Dr. Harold R. Henry

University of Arkansas
Technology Campus
P. O. Box 3017
Little Rock, AR 72203
ATTN: Paul C. McLeod

University of Arkansas
Mechanical Enginering
Fayetteville, AR 72701
ATTN: Jack H. Cole, Assoc Prof

Carnegie-Mellon University
Schenley Park
Pittsburgh, PA 15213
ATTN: Prof W. T. Rouleau, Mech Engr Dept

Case Western Reserve University
University Circle
Cleveland, OH 44106
ATTN: Prof P. A. Orner

The City College of the City Univ of NY
Dept of Mechanical Engineering
139th Street at Convent Avenue
New York, NY 10031
ATTN: Prof L. Jiji
ATTN: Prof G. Lowen

Duke University
College of Engineering
Durham, NC 27706
ATTN: C. M. Harman

Engineering Societies Library
345 East 47th Street
New York, NY 10017
ATTN: Howard Gordon

Franklin Institute of the State of Pennsylvania
20th Street & Parkway
Philadelphia, PA 19103
ATTN: Ka-Cheung Tsui, Elec Engr Div
ATTN: C. A. Belsterling

IIT Research Institute
10 West 35th Street
Chicago, IL 60616
ATTN: Dr. K. E. McKee

Lehigh University
Dept of Mechanical Engineering
Bethlehem, PA 18015
ATTN: Prof Forbes T. Brown

Linda Hall Library
5109 Cherry Street
Kansas City, MO 64110
ATTN: Documents Division

Massachusetts Institute of Technology
77 Massachusetts Avenue
Cambridge, MA 02139
ATTN: Engrg Tech Reports, Rm. 10-408
ATTN: David Wormley, Mech Engrg Dept, Rm. 3-146

Miami University
Dept of Engineering Technology
School of Applied Science
Oxford, OH 45056
ATTN: Professor S. B. Friedman

Michigan Technological University
Library, Documents Department
Houghton, MI 49931
ATTN: J. Hawthorne

University of Mississippi
201 Carrier Hall, Dept of Mech Engr
University, MS 38677
ATTN: Dr. John A. Fox

Mississippi State University
Drawer ME
State College, MS 39672
ATTN: Dr. C. J. Bell, Mech Engrg Dept

University of Nebraska Libraries
Acquisitions Dept, Serials Section
Lincoln, NE 68508
ATTN: Alan Gould

University of New Hampshire
Mech Engrg Dept, Kinsbury Hall
Durham, NH 03824
ATTN: Prof Charles Taft 3 copies

New Jersey Institute of Technology
Mechanical Engineering Department
323 High Street
Newark, NJ 07102
ATTN: Dr. R. A. Comparin

Ohio State University Libraries
Serial Division, Main Library
1858 Neil Avenue
Columbus, OH 43210

Oklahoma State University
School of Mech & Aerospace Engineering
Stillwater, OH 74074
ATTN: Prof Karl N. Reid

Pennsylvania State University
Dr. J. L. Shearer
215 Mechanical Engineering Building
University Park, PA 16802

Pennsylvania State University
Engineering Library
201 Hammond Building
University Park, PA 16802
ATTN: M. Bennett, Engineering Librarian

Purdue University
School of Mechanical Engineering
Lafayette, IN 47907
ATTN: Prof Victor W. Goldschmidt
ATTN: Prof Alan T. McDonald

Rock Valley College
3301 North Mulford Road
Rockford, IL 61101
ATTN: Ken Barton

Rutgers University
Library of Science & Medicine
New Brunsic, NJ 08903
Government Documents Dept
ATTN: Ms. Sandra R. Livingston

Syracuse University
Dept of Mech & Aerospace Engineering
139 E. A. Link Hall
Syracuse, NY 13210
ATTN: Prof D. S. Dosanjh

University of Tennessee
Department of Mechanical & Aerospace Engineering
Knoxville, TN 37916
ATTN: Asst. Professor G. Smith

University of Texas at Arlington
Mechanical Engineering Department
Arlington, TX 76019
ATTN: Dr. Robert L. Woods

University of Texas at Austin
Dept of Mechanical Engineering
Austin, TX 78712
ATTN: Dr. A. J. Healey

Tulane University
Dept of Mechanical Engineering
New Orleans, LA 70118
ATTN: H. F. Hrubecky

Union College
Mechanical Engineering
Schenectady, NY 12308
ATTN: Assoc Prof W. C. Aurbrey,
Mech Engrg Dept, Steinmetz Hall

Virginia Polytechnic Institute & State Univ
Mechanical Engineering Department
Blacksburg, VA 24061
ATTN: Prof H. Moses

Washington University
School of Engineering
P. O. Box 1185
St. Louis, MO 63130
ATTN: W. M. Swanson

West Virginia University
Mechanical Engineering Department
Morgantown, WV 26505
ATTN: Dr. Richard A. Bajura

Wichita State University
Wichita, KS 67208
ATTN: Dept Aero Engrg, E. J. Rodgers

University of Wisconsin
Mechanical Engineering Department
1513 University Avenue
Madison, WI 53706
ATTN: Federal Reports Center
ATTN: Norman H. Beachley, Dir.
Design Engineering Laboratories

Worcester Polytechnic Institute
Worchester, MA 01609
ATTN: George C. Gordon Library (TR)
ATTN: Technical Reports

AiResearch
P. O. Box 5217
402 South 36th Street
Phoenix, AZ 85034
ATTN: David Schaffer
ATTN: Trevor Sutton
ATTN: Tom Tippetts

Avco Systems Division
201 Lowell Street
Wilmington, MA 01887
ATTN: W. K. Clark 2 copies

Bell Helicopter Company
P. O. Box 482
Forthworth, TX 76101
ATTN: R. D. Yeary

Bendix Corporation
Research Laboratories Div
Bendix Center
Southfield, MI 48075
ATTN: Andrew Seleno
ATTN: C. J. Ahern

Bendix Corporation
Electrodynamics Division
11600 Sherman Way
N. Hollywood, CA 90605
ATTN: Mr. D. Cooper

Boeing Company, The
P. O. Box 3707
Seattle, WA 98124
ATTN: Henrik Straub

Bowles Fluidics Corporation
9347 Fraser Avenue
Silver Spring, MD 20910
ATTN: P. Bauer, Vice President/Engineering

Dr. Ronald Bowles
2105 Sondra Court
Silver Spring, MD 20904

Continental Can Company
Tech Center
1350 W. 76th Street
Chicago, IL 60620
ATTN: P. A. Bauer

Cordis Corporation
P. O. Box 428
Miami, FL 333137
ATTN: Stephen F. Vadas, K-2

Corning Glass Works
Fluidic Products, Houghton Park, B-2
Corning, NY 14830
ATTN: Mr. W. Schemerhorn
ATTN: V. S. Kumar

Chrysler Corporation
P. O. Box 118
CIMS-418-33-22
Detroit, MI 48231
ATTN: Mr. L. Gau

EMX Engineering, Inc.
354 Newark-Pompton Turnpike
Wayne, NJ 07470
ATTN: Anthony P. Corrado, President

Fluidics Quarterly
P. O. Box 2989
Stanford, CA 94305
ATTN: D. H. Tarumoto

General Electric Company
Space/RESD Divisions
P. O. Box 8555
Philadelphia, PA 19101
ATTN: Mgr Libaries, Larry Chasen

General Electric Company
Specialty Fluidics Operation
Bldg. 37, Room 523
Schenectady, NY 12345
ATTN: F. S. Ralbovsky, Fluidic Control
Products Engr

General Electric Company
Specialty Fluidics Operation
Building 37, Room 523
Schenectady, NY 12345
ATTN: R. C. Kumpitsch, Manager Fluidic Controls
ATTN: Mr. C. Ringwall

General Motors Corporation
Delco Electronics Divison
Manfred G. Wright
New Commercial Products
P. O. Box 1104
Kokomo, IN 46901
ATTN: R. E. Spaks

Grumman Aerospace Corporation
Technical Information Center
South Oyster Bay Road
Bethpage, L.I., NY 11714
ATTN: C. W. Turner, Documents Librarian

Honeywell, Inc.
1625 Zarthan Avenue
Minneapolis, MI 55413
ATTN: Dick Evans, MS S2658

Johnson Controls, Inc.
507 E. Michigan
Milwaukee, WI 53201
ATTN: Warren A. Lederman

Martin Marietta Corporation
Aerospace Division
P. O. Box 5837
Orlando, FL 32805
ATTN: R. K. Broderson, MP 326
ATTN: Vito O. Bravo, MP 326

Moore Products Company
Spring House, PA 19477
ATTN: Mr. R. Adams

National Fluid Power Association
333 North Mayfair Road
Milwaukee, WI 53222
ATTN: John R. Lueke
Dir of Tech Services

Richard White & Associates
Electro/Mechanical Engineers
77 Pelham Isle Road
Sudsbury, MA 01776
ATTN: Richard P. White

Rockwell International Corporation
Columbus Aircraft Division, P.O.Box 1259
4300 E. 5th Avenue
Columbus, OH 43216
ATTN: Mr. Marvin Schweiger

Sandia Corporation
Kirtland AFB, East
Albuquerque, NM 87115
ATTN: William R. Leuenberger, Div 2323

Stein Engineering Services, Inc.
5602 E. Monterosa
Phoenix, AZ 85018
ATTN: Mr. Peter Stein, President

United Technologies Research Center
400 Main Street
E. Hartford, CT 06108
ATTN: R. E. Olson, Mgr Fluid Dynamics Lab

Harry Diamond Laboratories
ATTN: McGregor, Thomas, Col., Commanding
Officer/Carter, W. W./Sommer, H.
Marcus, S. M., Technical Director
ATTN: Kimmel, S., PIO
ATTN: Chief, 0021
ATTN: Chief, 0022
ATTN: Chief, Lab 100
ATTN: Chief, Lab 200
ATTN: Chief, Lab 300
ATTN: Chief, Lab 400
ATTN: Chief, Lab 500
ATTN: Chief, Lab 600
ATTN: Chief, Lab 700
ATTN: Chief, Lab 800
ATTN: Chief, Lab 900
ATTN: Chief, Lab 1000
ATTN: Chief, 041
ATTN: HDL Library 3 copies
ATTN: Chairman, Editorial Committee 4 copies
ATTN: Chief, 047
ATTN: Tech Reports, 013
ATTN: Patent Law Branch, 071
ATTN: Chief, 340 10 copies
ATTN: Tadeusz Drzewiecki, 340
ATTN: Francis Manion, 340